Research Article

Fluvial dynamics in a deltaic environment under Little Ice Age intense climatic forcing (Bras de Fer, Rhône delta, France)

Anna Kharlanova[a] (iD), Claude Vella[a], Doriane Delanghe[a], Jules Fleury[a], Minoru Uehara[a], Véronique Rinalducci[b], Philippe Rigaud[b], François Demory[a], Kazuyo Tachikawa[a], Marta Garcia[a], Yoann Quesnel[a], Ghislain Gassier[a], Gaël Hemery[c], Edouard Bard[a] and Olivier Bellier[a]

[a]Aix-Marseille Université, CNRS, IRD, INRAE, Collège de France, CEREGE, Aix-en-Provence, France; [b]Aix-Marseille Université, CNRS, LA3M, Aix-en-Provence, France and [c]Société nationale de protection de la nature (SNPN), La Capelière – C134 de Fiélouse 13200 ARLES, France

Abstract

This study reconstructs the fluvial dynamics of the Bras de Fer distributary in the Rhône Delta (France) during the Little Ice Age (LIA) in response to short-term climatic forcing. A multiproxy approach combining historical cartography, sedimentology, geochemistry, magnetic susceptibility, and hydrological archives reveals accelerated meander migration and extensive overbank accretion between the late seventeenth and early eighteenth centuries CE. Increased flood frequency, coinciding with positive phases of the Atlantic Multidecadal Oscillation (AMO+), promoted rapid lateral channel shifts and the formation of crevasse splay complexes along the outside bank of the Grande Ponche meander. The results demonstrate that, despite stable relative sea levels, deltaic morphology remained highly sensitive to decadal-scale climatic variability, highlighting the dominant role of hydrological extremes in shaping fluvial-deltaic environments of Rhône delta during the late LIA.

Keywords: Rhône delta; Meander; Little Ice Age; Fluvial dynamics; Deltaic morphology; Overbank sedimentation; Crevasse splays; Geochemical analysis; Atlantic Multidecadal Oscillation

Introduction

In the context of contemporary climate change, rising sea levels and human pressures compromise the resilience of deltaic environments. A deeper understanding of the processes underlying delta formation is crucial for their preservation and sustainable development.

Deltaic morphology arises from the interplay between natural and human influences, mediated by the fluvial system's sediment supply, discharge, and intrinsic dynamics (Galloway, 1975; Boyd et al., 1992; Bhattacharya and Giosan, 2003; Bravard et al., 2008; Zolezzi et al., 2012). Variations in detrital input and hydrological parameters promote progradation or erosion (Passega, 1957; Wright, 1977; Schumm, 1981, 1985; Boyd et al., 1992; Dalrymple et al., 1992; Bhattacharya and Giosan, 2003). These processes are modulated by climatic (Bravard, 1989; Arnaud-Fassetta and Provansal, 1999; Goodbred, 2003; Clift and Jonell, 2021), eustatic (Stanley and Warne, 1994; Vella et al., 2005; Fanget et al., 2014), and tectonic variations (Colella, 1988). Human activities, such as deforestation and hydraulic engineering, have further altered sediment budgets and deltaic dynamics (Keesstra et al., 2005; Ericson

et al., 2006; Syvitski and Saito, 2007; Bravard et al., 2014; Anthony et al., 2015).

The Rhône Delta (Camargue, France) offers a pertinent case study, having undergone successive avulsions and rapid morphological changes during the late medieval and early modern periods (Arnaud-Fassetta, 1998; Arnaud-Fassetta and Provansal, 1999; Rey et al., 2005; Vella et al., 2005). Although these evolutionary phases are partly documented by historical sources (Pichard, 1995; Pichard et al., 2014; authors of this study, unpublished data), significant gaps remain regarding its modern period (Arnaud-Fassetta and Provansal, 1999; Arnaud-Fassetta, 2003), which this study addresses.

The Little Ice Age (LIA; fourteenth to mid-nineteenth century CE) was a period of climatic cooling, driven by reduced solar activity (Bond et al., 2001; Owens et al., 2017), increased volcanic activity towards the end of the LIA (Miller et al., 2012; Brönnimann et al., 2019), and changes in thermohaline circulation (Broecker, 2000). This resulted in more frequent and higher-magnitude flood events across European river systems (Carozza et al., 2012; Schulte et al., 2015; Perşoiu and Perşoiu, 2019). Within this context, the Bras de Fer distributary remained active from 1587 to 1711 CE, undergoing significant floods (Rossiaud, 1994; Arnaud-Fassetta and Provansal, 1999) and episodes of intense lateral accretion and progradation that contributed to one of the delta's latest expansion phases (authors of this study, unpublished data).

This study aims to reconstruct the morphodynamic evolution of the Grande Ponche meander—the most spatially extensive meander of the Bras de Fer— during the LIA through an integrated geomorphological, sedimentological, and geochemical approach. By examining extensive crevasse splay deposits and meander migration patterns, it seeks to highlight how short-term climatic variability affected deltaic morphology.

This study first outlines the palaeoenvironmental and hydrogeomorphological framework of the Bras de Fer channel, together with the geological and geomorphological context of the Rhône delta. It then examines the principal processes that shaped the channel's evolution during the LIA.

Palaeoenvironmental and hydrogeomorphological framework of the Bras de Fer channel

Geological setting

During the Holocene, the Rhône delta underwent several phases of progradation (L'Homer, 1975; Aloisi, 1986; Arnaud-Fassetta and Provansal, 1999; Rey et al., 2005, 2009; Vella et al., 2008) controlled by fluctuations in sea level (Vella et al., 2005; Stanford et al., 2011; Fanget et al., 2014; Fig. 1). Sediments accumulated over a Pleistocene gravel substrate following the deceleration of sea-level rise in the Mediterranean between 8000 and 6000 cal yr BP (Stanley and Warne, 1994). The Saint-Férréol and Ulmet lobes, comprising the ancient delta, emerged between approximately 4000 and 2000 cal yr BP (Vella et al., 2005). While the eastern and southern sectors of the delta plain developed during the medieval and modern periods (post-500 CE; Arnaud-Fassetta and Provansal, 1993), the southwestern part dates back to late antiquity and medieval times (post-100 BCE; Rey et al., 2005, 2009).

Geomorphological setting

Understanding the geomorphological evolution of the Rhône delta is fundamental to interpreting the sedimentary processes that shaped it. Extensive research has explored the geomorphology and sedimentology of the delta plain for the Holocene period (Duboul-Razavet and Duplaix, 1956; Suanez et al., 1998; Arnaud-Fassetta, 1998; Provansal et al., 2004; Arnaud-Fassetta et al., 2005; Vella et al., 2005, 2008; Martinez et al., 2024). Despite the availability of historical and archival data (Rossiaud, 1994; Caritey, 1995; Pichard, 1995; Landuré and Pasqualini, 2004; Pichard and Roucaute, 2014; Pichard et al., 2014), detailed information on the medieval and modern geomorphology remains limited (Arnaud-Fassetta and Provansal, 1999; Rey et al., 2005, 2009).

Holocene investigations have primarily targeted Roman antiquity (100 BCE–500 CE; Arnaud-Fassetta, 2000, 2002; Leveau, 2014; Vella et al., 2014, 2016) and the industrial period (post-1800 CE; Caritey, 1995; Sabatier, 2001; Antonelli, 2002; Maillet, 2005; Sabatier and Anthony, 2015; Boudet et al., 2017), leaving the LIA (~1300–1850 CE) comparatively understudied. Our research addresses this gap by reconstructing the evolution of the Bras de Fer distributary (1587–1711 CE) during the LIA, a period of active sediment supply and lobe construction (Arnaud-Fassetta and Provansal, 1999; Vella et al., 2005).

The delta's meandering style is driven by discharge, sediment load, topography, and from modern times, anthropogenic interventions (Arnaud-Fassetta and Provansal, 1999; Arnaud-Fassetta, 2002; Vella et al., 2005, 2014, 2016; Bravard, 2010). From the Middle Ages onwards, deforestation and changes in

land use increased sediment supply (Bravard, 1989, 2010). In the twentieth century CE, however, hydraulic constructions progressively reduced erosion and sediment transport, curbing delta progradation (Maillet et al., 2006; Besset et al., 2017).

The impact of the LIA on the Rhône delta remains poorly understood, particularly regarding overbank features such as crevasse splays. During this period, the delta exhibited a lobate or elongated morphology, driven by stable sea-level conditions and abundant sediment supply (Vella et al., 2005). Fluvial activity is reflected in overbank deposits, especially crevasse splays formed by levee breaches during floods (Russell, 1954; Coleman, 1969; Bridge, 2006; Yuill et al., 2016). Their extent depends on both allogenic (climate, discharge, sediment load) and autogenic factors (slope, sinuosity) (Millard et al., 2017; Rahman et al., 2022). The formation of crevasse splays often involves successive periods of flooding (Coleman, 1969; Millard et al., 2017), promoting progradation and possible avulsion (Smith et al., 1989; Slingerland and Smith, 1998).

In the Rhône delta, crevasse splays were previously documented during Roman times, with fine sandy deposits up to 70 cm thick (Arnaud-Fassetta, 2002). A contemporary example includes the 2003 CE breach of a dyke in the upstream part of the delta, leading to a crevasse splay covering approximately 429 ± 21 km^2 (Arnaud-Fassetta, 2013).

In the present study, extensive crevasse splays were identified along the outside bank of the Grande Ponche meander (Fig. 2), often exceeding 2 m in thickness. By combining granulometry, geophysics, geochemistry, historical cartography, and remote sensing, we reconstruct the LIA fluvial dynamics of the Rhône Delta at decadal resolution.

These geomorphological characteristics provide the basis for understanding the fluvial dynamics of the Bras de Fer channel during the LIA. The following section examines the hydrogeomorphological conditions that governed its activity, in particular the role of climatic variability and flood regimes.

Hydrogeomorphological settings of the Bras de Fer channel

During the LIA (~1300–1850 CE), the Rhône basin underwent significant hydrogeomorphological changes. Wetter phases favoured meander expansion and overbank flooding, while drier periods encouraged sediment deposition within channels, forming bars and islets (Bravard, 1989, 2010; Arnaud-Fassetta and Provansal, 1999; authors of this study, unpublished data). Historical cartography documents these fluctuations in delta geomorphology (Caritey, 1995; Arnaud-Fassetta, 1998; Pichard et al., 2014; authors of this study, unpublished data).

The Bras de Fer was active during a period of increased precipitation and flood frequency across the French Mediterranean region (Pichard, 1995). Enhanced runoff transported larger sediment volumes, fostering morphodynamic instability, channel shifts (Arnaud-Fassetta, 2003; Carozza et al., 2012), delta-lobe progradation (Arnaud-Fassetta and Provansal, 1999; Pichard et al., 2014), and morphological transformations (Bravard, 1989, 2010). Similar patterns were observed in other European river systems (Bellotti et al., 2004; Perşoiu and Perşoiu, 2019; Ruiz-Pérez and Carmona, 2019) and beyond (Seltzer and Rodbell, 2005).

Major flood events triggered the 1587 CE avulsion of the Grand Passon channel, redirecting flow through the Bras de Fer distributary (Rossiaud, 1994; Arnaud-Fassetta and Provansal, 1999). This shift was reinforced by enhanced sedimentation, resulting
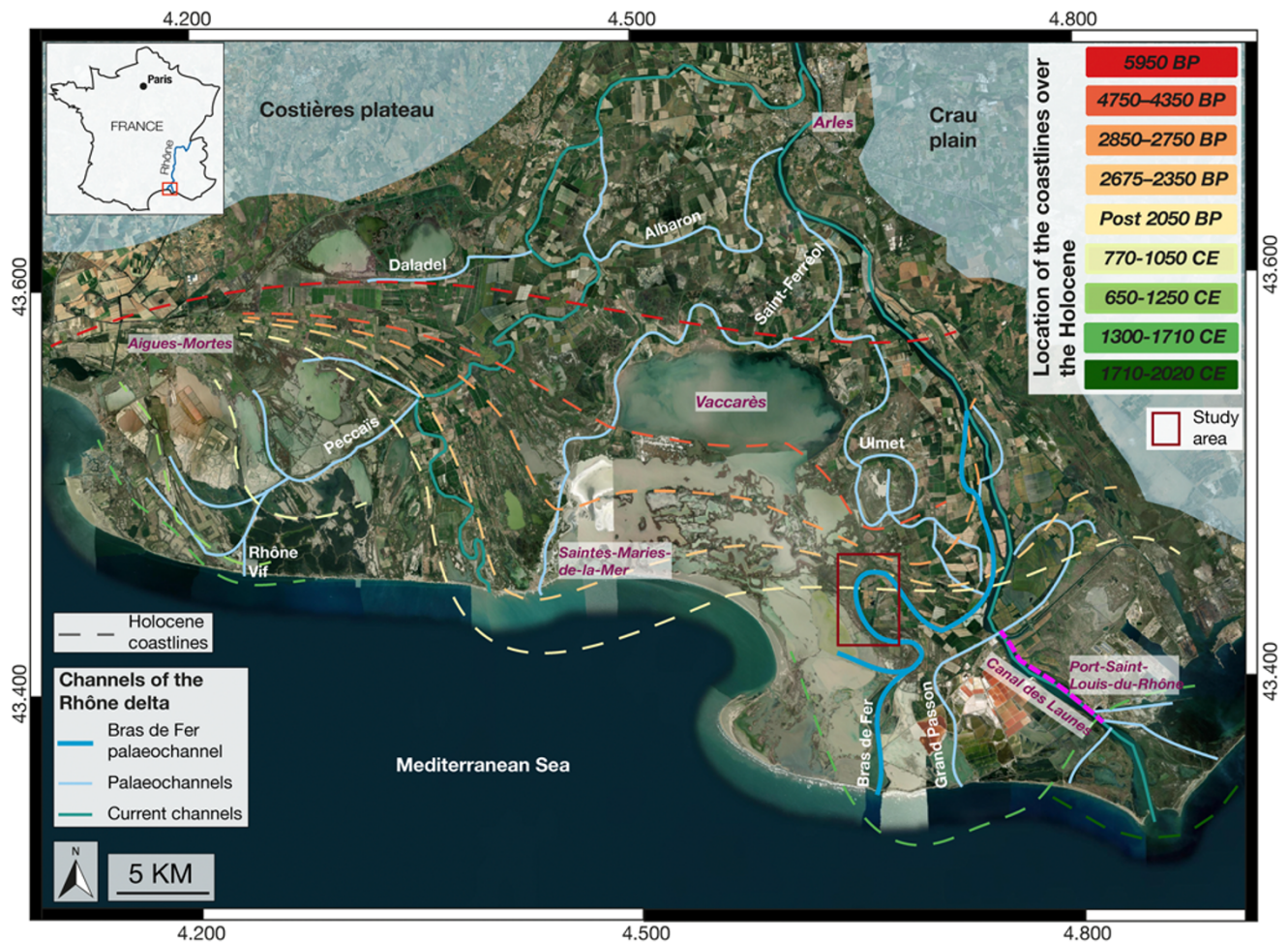
Figure 1. Holocene evolution of the three main Rhône delta lobes, based on palaeo-shoreline dating (L'Homer et al., 1981; Rey et al., 2005; Vella et al., 2008). This study focuses on the eastern channel, the Bras de Fer (highlighted in blue with a thick line). Satellite imagery: ESRI (2023).

from Alpine deforestation, overgrazing, and intense flood activity (Sclafert, 1959; Ladurie, 1967; Bravard, 1989; Arnaud-Fassetta, 1998; Pichard et al., 2014).

By the late 1600s and early 1700s CE, a high frequency of extreme floods (Pichard, 1995) remobilised sediments, driving delta progradation until the 1711 CE avulsion. This event interrupted sediment supply to the Bras de Fer mouth, initiating coastal erosion and sediment redistribution (Arnaud-Fassetta and Provansal, 1999; Pichard et al., 2014; authors of this study, unpublished data).

During the LIA, Mediterranean deltas such as the Rhône displayed a fluvial-dominated regime, contrasting with today's wave-dominated systems (Arnaud-Fassetta and Provansal, 1999; Bellotti et al., 2004; Ruiz-Pérez and Carmona, 2019).

Building on this hydrogeomorphological context, the next section focuses on the specific characteristics of the Grande Ponche meander, the key study area selected to reconstruct the fluvial dynamics of the Bras de Fer channel during the LIA.

Study area

This study examines the morphometric evolution of the Grande Ponche meander and the associated overbank deposits along its outside bank. The area was selected for its well-preserved palaeolandforms of lateral sedimentation (Fig. 2B), which have remained relatively undisturbed due to limited agricultural activity and protection within a regional natural park.

The Grande Ponche is one of four meanders along the Bras de Fer, whose amplitude declines seaward (Fig. 2A). According to Schumm's (1981, 1985) classification, this reach is close to a low-stability meandering channel due to its gentle slope, fine sediment load, wide meander bars, and increased channel width at apices.

The northernmost meander (no. 1, in red in Fig. 2A) is circular and almost symmetrical, situated in an area heavily modified by agriculture and intersected by palaeochannels (Ulmet, Grand Passon, and Bras de Fer).

The Grande Ponche meander (no. 2), which is symmetrical and elongated (Fig. 2A), shows a chute cutoff, downstream shifting, and well-preserved overbank deposits, including topographically pronounced crevasse splays, which likely capture the dynamics of intense flood episodes. These deposits are expected to contain coarser sediments due to higher shear stress and velocities on the outside bank (Clayton and Pitlick, 2007). Sedimentation on the inside bank, documenting the channel's active phase and infilling, was previously described by Arnaud-Fassetta and Provansal (1999) (core sample locations in green in Fig. 2B).
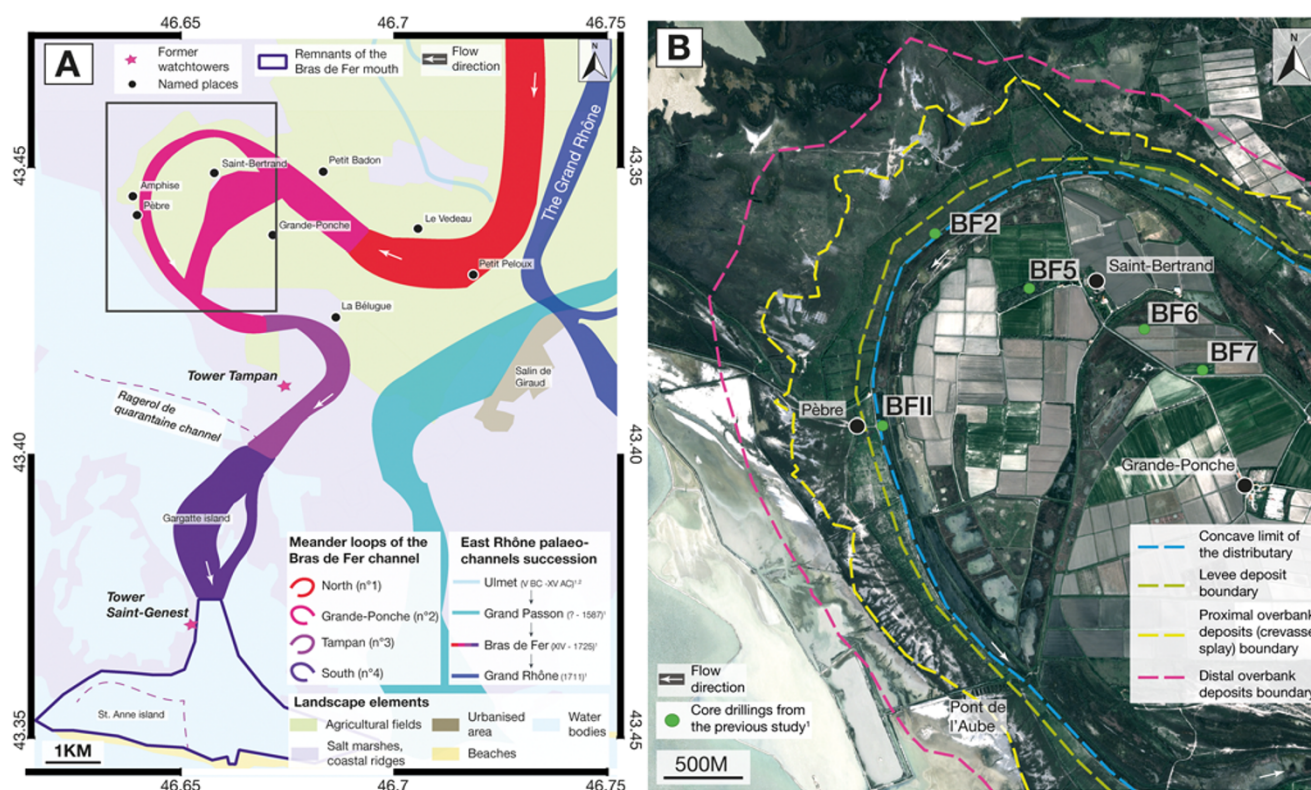
Figure 2. (**A**) Four meanders of the Bras de Fer and associated landscape features, with the study area outlined. Sources: 1, Arnaud-Fassetta (1998); 2, Vella et al. (2016); (**B**) Pléiades (CNES 2023) satellite image of the study area (**A**), showing continuous fossil outside overbank deposits of the Grande Ponche meander. Boundaries of lateral deposits (dashed lines) derived from a digital terrain model (DTM). Green dots indicate drill core locations from a previous study conducted by Arnaud-Fassetta (1998).

These first two meanders likely began forming when the Bras de Fer became the main distributary, or possibly earlier, during the final activity of the Grand Passon. It may have recorded multiple phases of flood intensification and reduction.

The Tampan meander (no. 3) is less developed and slightly asymmetrical, featuring several internal bars (Fig. 2A). Historical cartography suggests it formed later than the Grande Ponche, likely during a short period of large floods in the second half of the seventeenth century CE.

A fourth, subtle meander (no. 4 in Fig. 2A), marks the onset of sinuosity along an otherwise straighter reach, active between the mid-seventeenth and early eighteenth centuries CE, before the Rhône's 1711 CE avulsion.

Methodology

Morphometric evolution of the Grande Ponche meander using ancient maps and aerial images

Historical maps containing at least four stable landmarks (e.g., towers, farmsteads) were georeferenced using thin plate spline transformations (authors of this study, unpublished data). Early or distorted maps lacking sufficient control points were nonetheless utilised for descriptive purposes. Two undated maps were provisionally dated based on cartographic features and comparison with documented meander dynamics.

Recent spatial data supplemented interpretations, including 1942 aerial photographs ("C2942-0011_1942_NIMES-CAMARGUE" [IGN, 1942]). These photographs were orthorectified into mosaics, capturing morphologies later modified by agriculture.

Morphometric properties and estimation of meander migration

The morphological evolution of the Grande Ponche meander was reconstructed using historical maps (Supplementary Table 1) and 1942 imagery. Standard morphometric parameters were calculated: sinuosity (S), wavelength (λ), amplitude (A), radius of curvature (Rc), and channel width (W) (Leopold and Wolman, 1957; Hooke, 1984, 2013; Knighton, 1998).

The Rc/W ratio indicates meander dynamics: 4–20 suggests growth, 2–3 denotes active migration, and <2 implies chute cut-off or abandonment (Bagnold, 1960; Hey, 1984; Hooke, 1997). Meander expansion rates were calculated based on changes in Rc across dated intervals, and lateral extension was assessed from apex migration relative to elapsed time. Bankfull discharge (Q_b) and annual peak flood discharge ($Q_{1.58}$) were estimated using Dury's equations (1955, 1976).

Although the fossilised and partially modified state of the channel may introduce uncertainties, these estimates provide valuable insights into its historical dynamics.

Interpretation of overbank deposits using a digital terrain model

A 50-cm-resolution digital terrain model (DTM) was created from a LIDAR HD (IGN 2022) point cloud and processed using R Studio scripts to retain only terrain returns, then interpolated into

a triangulated irregular network surface. The original density of 10 points/m² (compared with 1 point/m² in previous datasets [SHOM, 2015; IGN, 2018]), allowed detection of subtle features like crevasse splays, levees, and crevasse channels.

The DTM was used to target depositional forms for in situ stratigraphic surveys, sedimentological analyses, and geophysical investigations.

Sedimentary analysis

Stratigraphic data from three trenches, eight cores, and multiple auger samples were used to reconstruct depositional episodes. Among various sedimentary parameters, grain size and isothermal remanent magnetisation (IRM) intensity were selected as key indicators for depositional environments.

Grain-size analysis

Samples were taken at facies changes. Carbonates and organic matter were removed using HCl (35%) and H_2O_2 (30%) (for protocol, see Sharifi et al. [2018] and Lepage et al. [2019]). Grain-size distributions were measured by laser diffraction (Beckman Coulter LS 13 320, Malvern Mastersizer 3000). Both instruments detect particles from ~0.04 to 2000 µm. The Blott and Pye (2012) classification scheme was adopted, with clay (<3.91 µm) grouped into a single class due to its low abundance (<10%). Results were presented as bar charts and median grain-size distributions by facies. Depositional hydrodynamics were further characterised using a Passega (1957, 1964) CM diagram, which correlates coarsest percentile (C) with median size (M) to characterise depositional hydrodynamics.

Detailed information on the calibration protocols and data variability between instruments can be found in Supplementary Material 1.

IRM intensity

U-channels were magnetised using a 0.6 T Halbach cylinder to impart IRM, then scanned at high resolution (500 µm) with a fluxgate-based device (Demory et al., 2019). This process mobilises most ferromagnetic particles, mainly iron oxides and hydroxides typical of oxic sediments (Scheidt et al., 2017).

Sensitive to detrital input, IRM serves as a proxy for reconstructing fluvial dynamics. The scanner's centimetre-scale resolution allows precise correlation of magnetic signals with sedimentary facies, refining environmental reconstructions (Demory et al., 2019).

Elemental composition and radiography

Elemental composition and sediment radiography were obtained using high-resolution X-ray fluorescence (XRF) scanning (ITRAX, Cox Analytical Systems) on U-channels with a Mo tube as the X-ray source. Scanning at 2 mm intervals (30 kV, 40 mA, 15 s count) provided intensity profiles of terrigenous elements (Fe, Ti, Si, K, Zr) and carbonates (Ca). Radiographic imaging (45 kV, 40 mA, 400 ms exposure, 200 µm resolution) simultaneously delivered density-contrast data, enhancing the detection of sedimentary structures beyond visual descriptions (Croudace et al., 2006).

Geochemical proxies supported palaeoenvironmental reconstructions. Zr/Rb ratios served as a grain-size proxy: higher values indicate coarser, flood-transported material (Turner et al., 2015; Talská et al., 2021), with zirconium mainly sourced from the Massif Central in the Rhône delta (Arnaud-Fassetta and Provansal, 1999).

Ca/Si distinguished carbonate from siliceous inputs: high Ca values mark carbonate-rich flood deposits, whereas high Si denotes silicate-dominated sources (Schulte et al., 2015). Both elements are thus exploited here as tracers of high-energy events.

Si/K acted as a proxy for the siliceous-to-clay content ratio, with higher values indicating sandy sediments and lower ones marking clay-rich deposits. Potassium, associated with clays, signals increased fine-grained sediment supply during floods (Schulte et al., 2015).

Subsurface stratigraphy by electrical resistivity tomography and trenches

Electrical resistivity tomography (ERT) is a non-invasive technique for mapping subsurface resistivity variations (Maillet et al., 2005; Florsch and Muhlach, 2018), effective in studying alluvial deposits (Maillet et al., 2005; Laigre et al., 2012; Salomon et al., 2016; Bellmunt et al., 2022).

Resistivity is influenced by sediment composition, water content, texture, clay content, and porosity (Rhoades et al., 1989). In saturated sandy zones, lower values are common, especially near the water table (~0 m depth).

Nine ERT profiles were acquired across the Grande Ponche overbank deposits using an ABEM Terrameter SAS4000 (Schlumberger-Wenner array, 0.5–1 m electrode spacing), reaching depths of up to 8 m. Data were processed with RES2DINV (Geotomo). Stratigraphic observations from trenches validated and refined the geophysical interpretations.

Radiocarbon dating procedures

Radiocarbon dating was performed on bulk organic matter and gastropod shells from trenches. Calibrations used Calib Rev 8.1.0 software (Reimer et al., 2020) and the IntCal20 curve. Results are expressed in calibrated years BP (2σ range), detailed in Supplementary Table 3.

Results

Morphometric evolution of the Grande-Ponche meander

An analysis of 15 historical maps (Supplementary Table 1) implies that the Grande Ponche meander developed during the Bras de Fer's period of activity as the main distributary, potentially becoming significant before the avulsion event. The 1593 CE map, the earliest to show the meander, indicates an established channel, possibly initially a secondary one.

Throughout the seventeenth century CE, the meander migrated laterally, evidenced by shifting toponyms and islet formation along the inside bank. After 1688 CE, migration accelerated, with prominent scroll bar development and increasing distance between the active bank and the Grande Ponche farmhouse (Fig. 3, Supplementary Fig. 1).

Georeferencing enabled the repositioning of the former channel on 1942 imagery (Fig. 3), allowing morphometric tracking (Supplementary Table 2). Sinuosity (S) increased from 1.7 in 1635 CE to 2.5 before the chute cutoff; amplitude (A) expanded from 2.8 km to 5.4 km. Meanwhile, the radius of curvature (Rc) remained stable at 1.4 km, while channel width (W) fluctuated between 0.42 and 0.80 km, narrowing before abandonment.

Between 1635 and 1688 CE, the meander rotated approximately 50° and migrated 1.4 km southwards, with a further 0.3 km migration recorded before flow cessation (Fig. 3). Around 1700 CE, a chute cutoff formed the Isle of Saint-Bertrand (Fig. 3C, Supplementary Fig. 2). Later eighteenth-century CE maps depict flow diverted into the Canal des Launes (thick fuchsia dashed line in Fig. 1), relegating the Bras de Fer to a secondary channel (Supplementary Fig. 3) until its fossilisation (Fig. 3D). By 1754 CE,
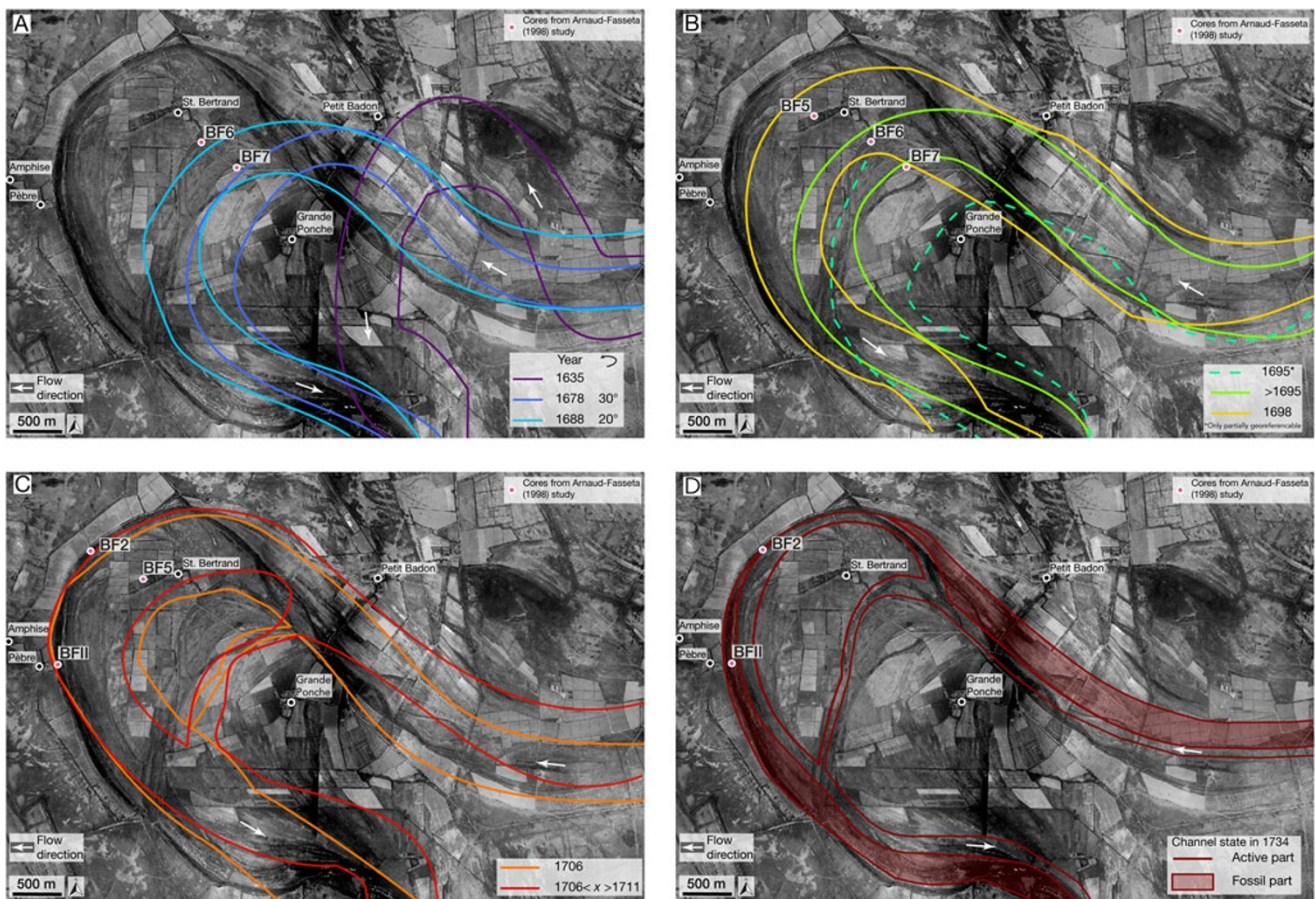
Figure 3. Evolution of the Grande Ponche meander (1635–1734 CE) based on georeferenced historical maps over 1942 aerial photographs (IGN Remonter le temps, 1942). (**A–C**) Gradual shift and increasing curvature of the meander (1635–1706 CE). (**D**) Post-avulsion phase and onset of fossilisation. Core samples from Arnaud-Fassetta (1998) are marked in pink.

the Bras de Fer had become reduced to ∼1 m depth and 32 m width at the northern meander (Supplementary Table 1).

The Rc/W ratio fluctuated between 1.8 and 3.3, peaking in 1678 CE, stabilising around 2.2–2.3 (1688–1690 CE), and declining to 1.8 by 1695 CE. It rose sharply after the chute cutoff and avulsion. Migration rates were negligible until 1695 CE, then surged briefly before decreasing again post-cutoff. Apex extension rates were positive in the late seventeenth to early eighteenth centuries CE, turning negative after partial abandonment (Supplementary Table 2).

The bankfull discharge (Q_b), along with the most probable annual flood ($Q_{1.58}$) also increased during the late seventeenth and early eighteenth centuries CE, reaching Q_b ∼16,147 m³/s (1699 CE) and $Q_{1.58}$ ∼44,995 m³/s (by 1734 CE), estimated using Dury's equations. The chute cutoff development led to a decline, with Q_b dropping to 11,806 m³/s in 1706 CE (Supplementary Table 2). Given data and method uncertainties, these variations represent indicative trends rather than significant changes.

Detection of overflow forms on the outside bank of the Grande Ponche

The high-resolution DTM of the Grande Ponche meander's outside bank reveals extensive crevasse splay deposits at Amphise, Pèbre, and Pont de l'Aube (Fig. 4).

At Amphise, crevasse splays are broad, with a main channel and few secondary channels. At Pèbre, they are narrow, coalescing, and dendritic (Fig. 4). At the Pont de l'Aube (Fig. 5A), crevasse splays are wider, less elongated, and associated with a complex distributary network. Proximal deposits along the outside bank are coarser, while distal deposits are finer and flatter, marking the transition to the floodplain (Fig. 5A).

The DTM (50 cm resolution) further identifies microtopographies within the crevasse splays, such as channels, microlevees, and channel lobes developing within depressions (Fig. 5A). Vegetation differences further aid discrimination: the normalized difference vegetation index analysis from May 2015 Pleiades imagery highlights strong contrasts in chlorophyll activity, with higher values on levees populated by *Tamarix gallica* and lower in crevasse splays dominated by *Salicornia* (Supplementary Fig. 4).

ERT surveys (Fig. 5B) corroborate these findings, suggesting distinct resistivity contrasts: higher values on levees, moderate in channels, and lower on floodplains. Each profile uses a distinct resistivity legend to preserve interpretative accuracy, with values considered relative.

Profiles a-d (Fig. 5B) distinguish two main units: an upper, resistive sandy layer and a lower, conductive silty unit. High resistivity corresponds to sandy, dry levees; intermediate values reflect crevasse splays; and the lowest values mark saturated floodplain
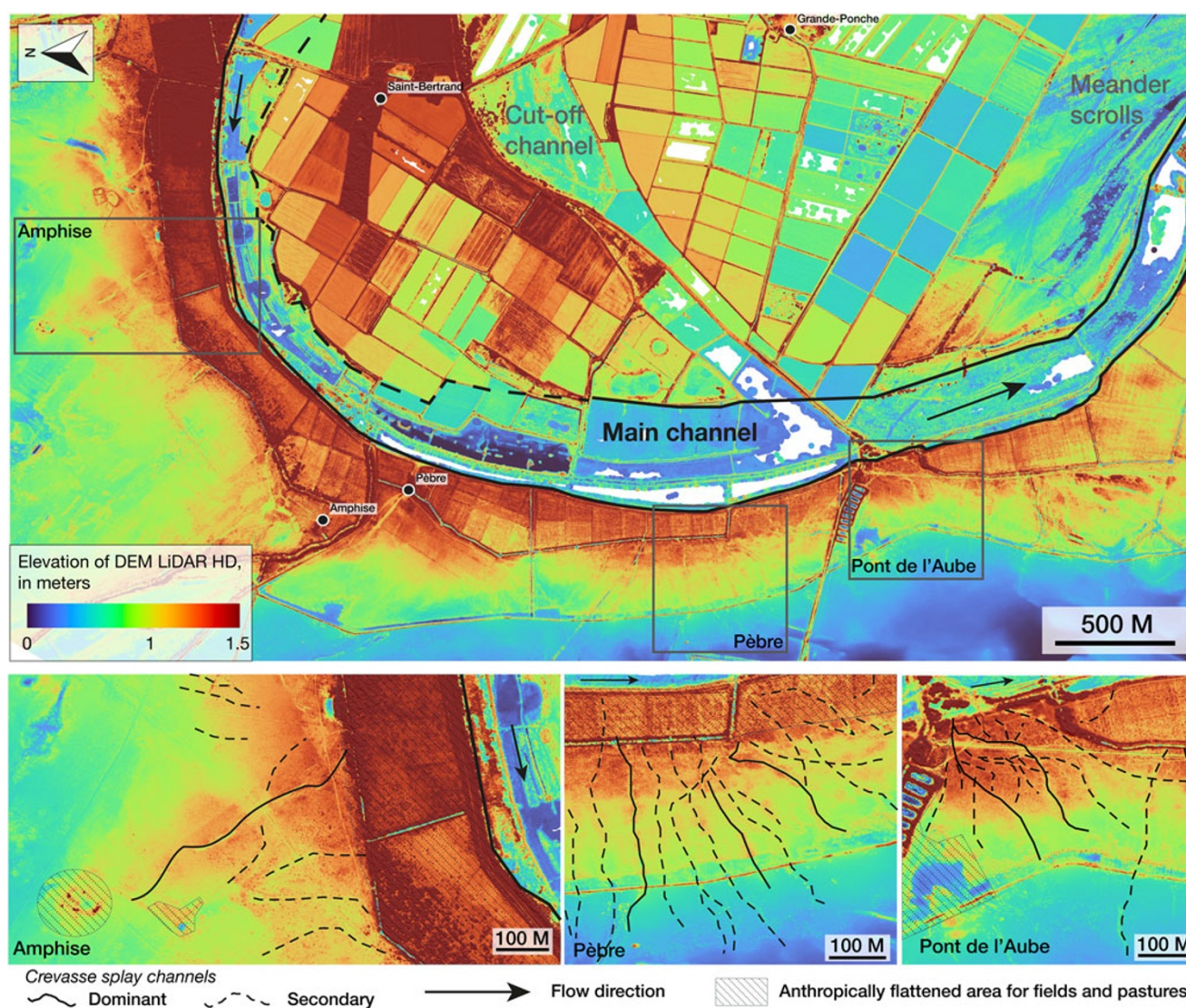
Figure 4. Crevasse splay deposits along the outside bank of the Grande Ponche meander (Bras de Fer) on a 50-cm high-resolution digital terrain model (DTM) (IGN, 2022). Deposit extents outlined in black; areas anthropogenically levelled indicated by diagonal dashed lines at Amphise, Pèbre, and Pont de l'Aube.

deposits. These results are consistent with sedimentological observations from cores and trenches (Figs. 6 and 7).

Identification of depositional environments based on sedimentological analysis

Sediment cores (Fig. 6) and trench exposures (Fig. 7) reveal three main fluvial facies: floodplain, levee, and crevasse splay deposits, differentiated through grain-size distributions, geochemical ratios (Zr/Rb, Ca/Si, Si/K), and IRM intensity (Figs. 8 and 9).

Lagoon environment

Beneath fluvial sequences, a basal lagoonal unit, dated between 899–1042 CE (Amphise) and 943–1026 CE (Pont de l'Aube), comprises fine sands (125–500 μm) and bluish clay-silts (Fig. 10). It is characterised by low Zr/Rb and Ca/Si ratios, weak IRM intensities, and high Si/K, indicative of low-energy, siliceous sedimentation (Fig. 8). Mollusc assemblages (e.g., *Cerastoderma edule, Bittium*

reticulatum) and thin laminae further indicate low-energy lagoonal conditions.

Fluvial environment

Above the lagoonal deposits, overlying fluvial sediments demonstrate spatial and stratigraphic heterogeneity, reflecting flow dynamics.

Floodplain deposits. Floodplain facies mainly comprise laminated clay-silts with subhorizontal to gently inclined bedding (<15°) (Figs. 6 and 7). They exhibit low Zr/Rb and Si/K ratios, reduced IRM intensities, and slightly elevated Ca/Si ratios compared with other facies (Figs. 8 and 9), attributed to diminished silica-rich input and relative calcium enrichment of detrital origin, given the lack of ostracods. Radiographic images reveal thin graded layers and minimal bioturbation (Figs. 8 and 9). The fine-grained texture and high water content correspond to low resistivity (<1.5 ohm·m) in ERT profiles (Fig. 5B). Fine laminations, colour, oxidation traces, and fauna distinguish floodplain deposits from lagoonal facies (Fig. 7).
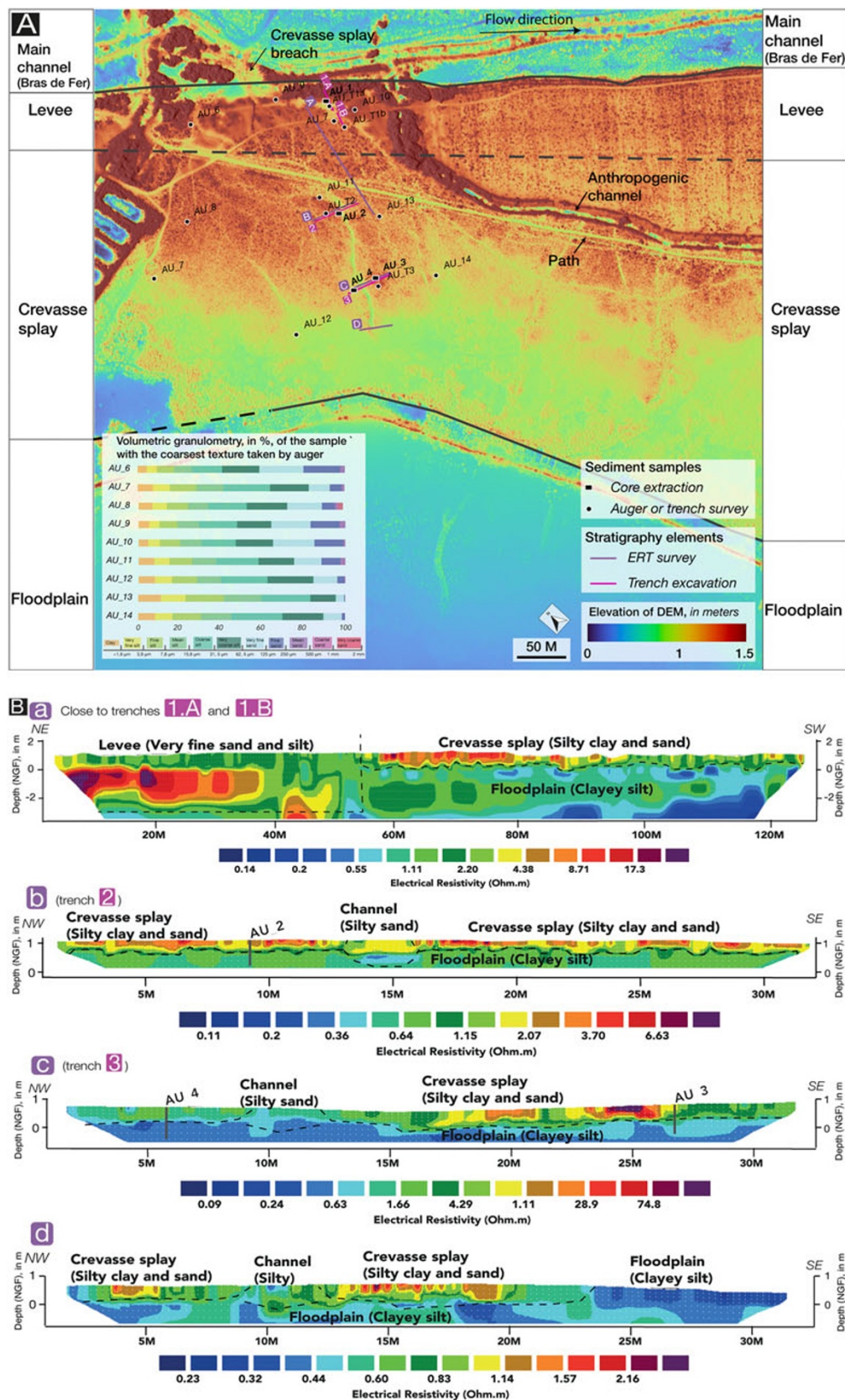
Figure 5. (**A**) A 50-cm high-resolution digital terrain model (DTM) showing the topography of overbank deposits on the outside bank at the Pont de l'Aube, with locations of trenches, electrical resistivity tomography (ERT) profiles, and results of granulometric sampling indicating the coarsest sediments at each site. (**B**) ERT profiles across lateral overbank deposits of the Grande Ponche meander: one along the levee to crevasse splay transition (**A**) and three perpendicular to the main crevasse splay channel (**B–D**). Profile locations shown in **A**. Each profile has a unique resistivity legend to preserve interpretative accuracy. Standardizing these legends would obscure significant variability;. NGF, Nivellement Général de la France (French national vertical datum). (French national vertical datum)
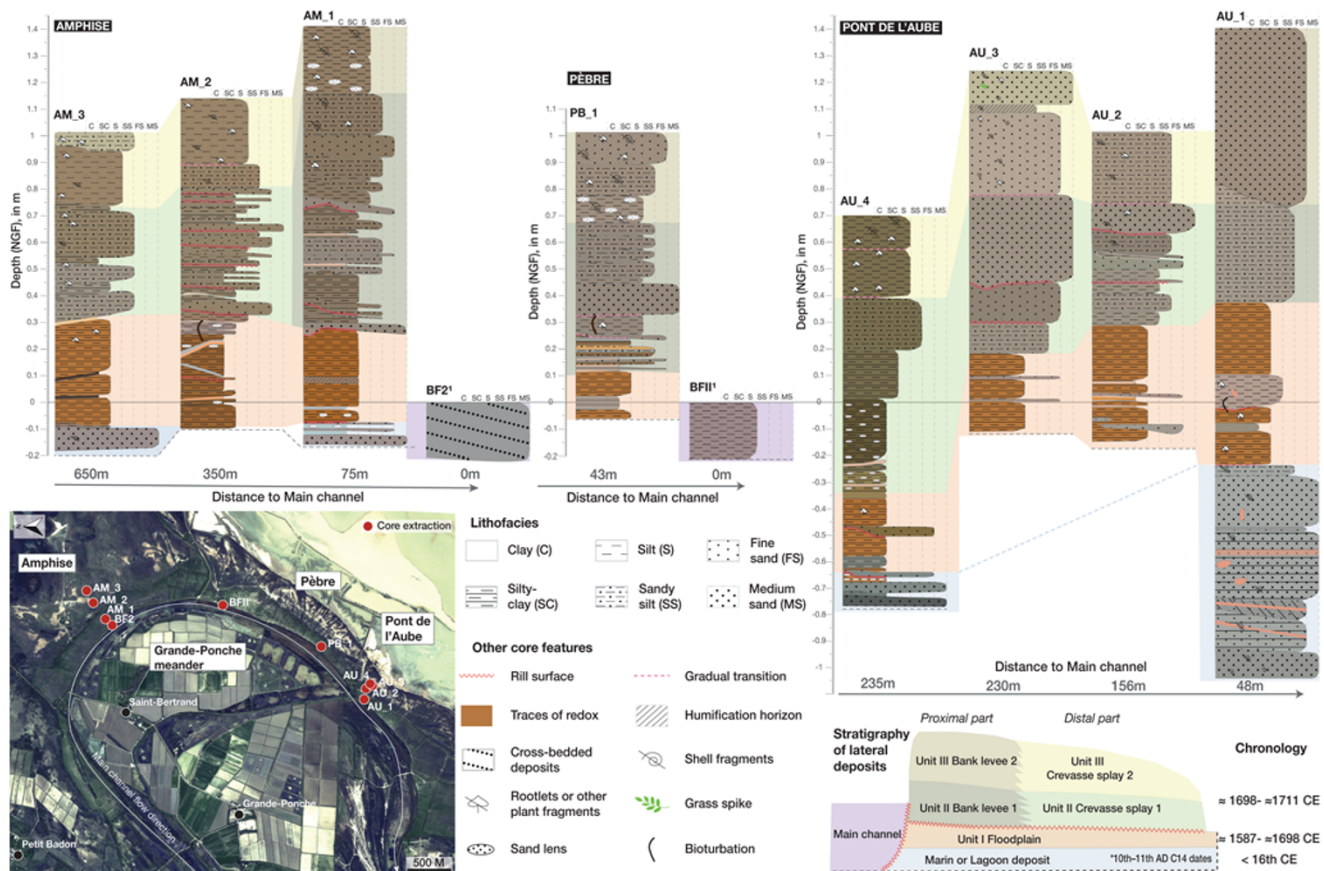
Figure 6. Cores taken from overbank deposits on the outside bank of the Grande Ponche meander, both in the proximal parts, on the levee (AM_1, PB_1, AU_1), and in the distal parts, on the crevasse splays (AM_2, AM_3, AU_2, AU_3, AU_4), as well as two channel cores (BFII, BF2), taken by Arnaud-Fassetta (1998). Overflow deposits reveal three fluvial units consistently identified across proximal and distal areas: basal floodplain deposits overlain by levee or crevasse splay sediments, each subdivided into a bedded, heterogeneous facies (phase 1) and a massive, homogeneous facies (phase 2).

Overbank deposits: levee and crevasse splay. Overbank deposits vary with channel proximity. Proximal levee deposits (core AM_1 [Fig. 9]; trenches 1.A and 1.B [Fig. 7]) display inverse grading, current ripples, and oblique bedding enriched in coarse silt (15.6–31.5 µm) (Figs. 5A, 7, and 10), with elevated Zr/Rb and Ca/Si ratios (Fig. 9), reflecting high-energy floods and detrital carbonate input. Si/K ratios increase in sandy intervals and decline in finer layers, indicating hydrodynamic variations (Fig. 9). Distal crevasse splay deposits (cores AM_2 and AM_3) are finer grained and laminated, and show a downstream decline in elemental intensities derived from XRF measurements, consistent with progressive sedimentary fining away from the channel (Figs. 5A, 7, and 9). The absence of ostracods throughout confirms an azoic depositional environment, with carbonate inputs considered detrital.

Both levee and crevasse splay deposits can be subdivided into two depositional phases:

1. **Phase 1** consists of coarser, heterogeneous beds with frequent inverse grading and a broad grain-size range (fine silt to fine sand) (Figs. 5A, 7, and 10). This phase is marked by higher Zr/Rb and Ca/Si ratios (Fig. 9).
2. **Phase 2** comprises finer, more homogeneous silt-dominated beds (Figs. 7 and 10), with markedly lower Zr/Rb and Ca/Si ratios (Fig. 9). IRM intensities increase slightly relative to phase 1 (Fig. 9), due to the relative enrichment in fine magnetic minerals as coarse quartz and carbonate particles diminish.

Although ERT profiles (Fig. 5B) do not resolve both phases precisely, they distinguish higher-resistivity levees, intermediate crevasse splays, and low-resistivity floodplain units.

Sub-environments of crevasse splay deposits

Crevasse splays are complex internal structures, including shallow distributary channels and small channel–levee systems (Figs. 5A and 7). Several stacked channel fills alternate coarse sand and silt sequences, overlain by flood-silt drapes and separated by subtle erosional contacts (Fig. 7).

ERT profiles occasionally detect near-surface crevasse channels as localised resistivity minima, although deeper lags are rarely discernible due to thinness and lithological similarity to surrounding deposits (Fig. 5B).

The crevasse channels are dominated by fine sands (125–250 µm), with smaller peaks in medium and coarse silts (Figs. 7 and 10). Channel–levee units contain the coarsest material, with more than 40% fine sand in phase 1, while phase 2 becomes more silt dominated (Fig. 10).

Climbing ripples and other current structures, typical of crevasse splay environments (Gulliford et al., 2017), were observed in trenches, with gentle dips towards the northeast–southeast (Fig. 7).

Sedimentary structures and geochemical signals collectively denote repeated episodes of large overbank flooding, followed by
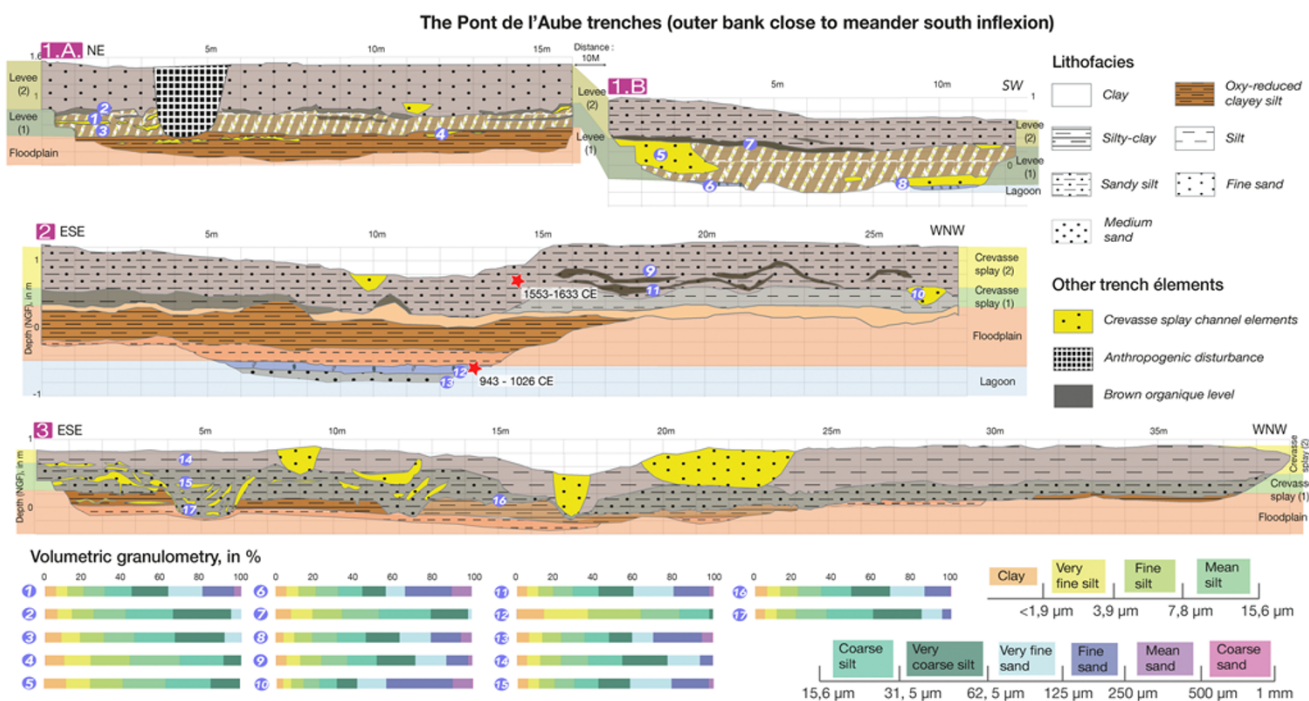
Figure 7. Stratigraphic cross sections showing the chronology and grain-size distribution of levee, crevasse splay, and floodplain deposits at Pont de l'Aube (location in Figure 5A). Radiocarbon (^{14}C) dates from trench samples are marked with red stars, calibrated with Calib Rev 8.1.0 (Reimer et al., 2020) using the IntCal20 curve. Radiocarbon dates agree broadly with archival records. A lagoon-to-fluvial transition (943–1026 CE) predates the documented Bras de Fer period of activity, while a later date (1553–1633 CE) precedes the major depositional phase, possibly reflecting reworking or local sediment pulses. NGF, Nivellement Général de la France (French national vertical datum). (French national vertical datum).

waning flow phases across the outside bank of the Grande Ponche meander.

Characterisation of depositional processes on the outer bank of the Grande Ponche meander: geochemical and magnetic signatures and transport dynamics

The k-means clustering results, projected onto the principal component analysis (PCA) plane, reveal four distinct groupings that correspond to specific sedimentary facies (Fig. 11). The k-means classification divides samples into clusters based on similarity (Hartigan and Wong, 1979), while PCA reduces data dimensions to point out key variations (Jolliffe and Cadima, 2016). By applying PCA to the k-means results, we reduce high-dimensional geochemical data to two dimensions, enabling clear visualization of the clusters. Lagoonal–marine sands are well isolated in cluster 2, showing clear geochemical distinction from fluvial facies. Floodplain deposits dominate cluster 4, while clusters 1 and 3 contain a mix of levee and crevasse splay samples, reflecting their compositional overlap. Most misclassifications occur among fluvial facies, where certain laminae share similar characteristics.

The Passega CM diagram (Fig. 12) further highlights two main depositional modes at the Grande Ponche outer bank. Floodplain and phase 2 of crevasse splay and levee deposits plot in the T and lower RS fields, indicating low-energy suspension settling. Phase 1 crevasse splay samples extend into the upper RS and QR fields, indicating higher-energy flood events. All facies occur within the RS field, while samples near the QR boundary mark crevasse channel and phase 1 crevasse splay deposition.

Interpretation

An analysis of historical cartography, sedimentary sequences, geophysical surveys, and geochemical proxies demonstrates that the Grande Ponche meander underwent rapid lateral migration and important overbank deposition between 1660 and 1710 CE. Three key observations underpin this interpretation:

1. Hydromorphological instability triggered by climatic variability. Historical maps highlight an acceleration of meander migration (Fig. 3, Supplementary Table 2), up to 26 m/yr between 1684 and 1700 CE (Fig. 13), coinciding with peaks in flood frequency (Fig. 14). The decline of the *Rc/W* ratio (Fig. 14) below the stability threshold (Bagnold, 1960; Hey, 1984; Hooke, 1997), together with the documented outside bank accretion (Fig. 4), reflects instability and a transition towards the chute cutoff.

   Application of Dury's formula (Fig. 14) provides bankfull discharge estimates above 10,000 m^3/s for the Grande Ponche meander, consistent with the Rhône's largest historical floods (12,500 m^3/s in 1856; 11,500 m^3/s in 2003; Levraut and Roy, 2007) and far exceeding the Rhône's present-day mean annual discharge (~1680 m^3/s; Hydro.eaufrance, n.d.). Deforestation and land-use changes (Bravard, 1989, 2010) likely enhanced sediment flux.

   This frequent flood period aligns with positive phases of the Atlantic Multidecadal Oscillation (AMO+) (Gray et al., 2004; Mann et al., 2009; Knudsen et al., 2014), characterised by increased precipitation extremes and altered wind patterns (Curtis, 2008; O'Reilly et al., 2017). The synchronicity between AMO+ phases and heightened Rhône fluvial activity (Fig. 14) supports the influence of decadal climatic oscillations, potentially
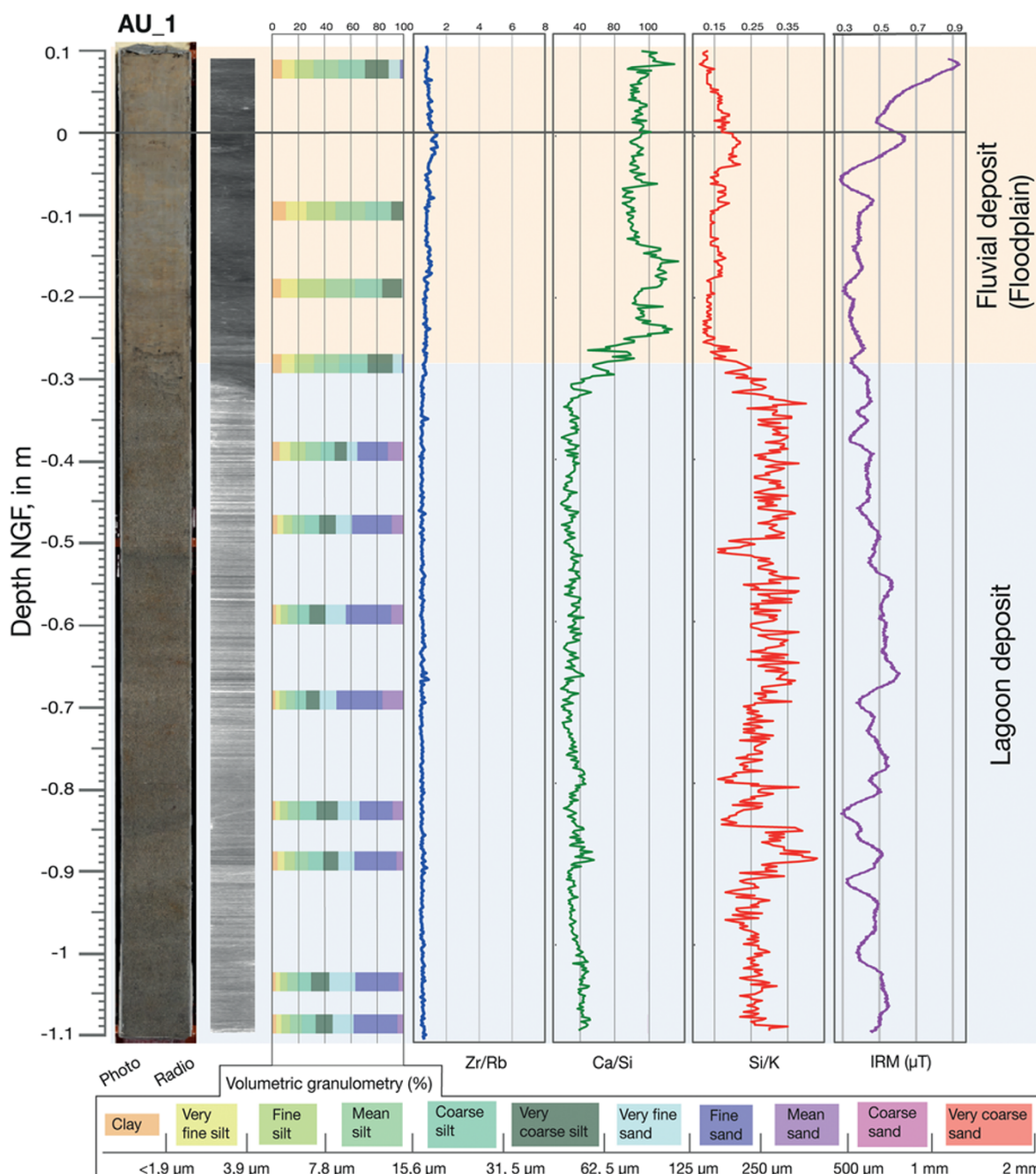
Figure 8. Core AU_1 from the base of trench 1.A (location shown in Figure 5A), with log showing photograph, radiography, volumetric granulometry, elemental ratios (Zr/Rb, Ca/Si, Si/K), and isothermal remanent magnetisation (IRM) intensity. The figure illustrates the distinction between fluvial (floodplain) and lagoon deposits. NGF, Nivellement Général de la France (French national vertical datum). (French national vertical datum)

amplified by the Maunder Minimum and enhanced volcanism (Miller et al., 2012; Brönnimann et al., 2019) around 1700–1710 CE.

2. Extensive crevasse splay deposits indicative of multiple bank breaching.

   Crevasse splay deposits detected along the outside bank reflect repeated natural levee breaches during large floods (Fig. 4). As detailed in "Identification of Depositional Environments Based on Sedimentological Analysis," the overbank deposits exhibit a dual-phase organisation: phase 1, comprising coarse, heterogeneous beds deposited under high-energy conditions during flood surges; and phase 2, consisting of finer, more homogeneous silts laid down during declining flow energy. Elevated Zr/Rb and Ca/Si ratios in phase 1 confirm intense detrital input during peak flooding. Their decline in phase 2, along with a slight increase in IRM values, points to finer sedimentation and a relative enrichment in magnetic minerals as coarse inputs diminish.

   These facies may represent either distinct floods or the front- and back-loading phases of singular flood events, as suggested by Filgueira-Rivera et al. (2007). Fine-grained phase 2 deposits may also reflect channel abandonment processes or distal overbank sedimentation (Gulliford et al., 2017).
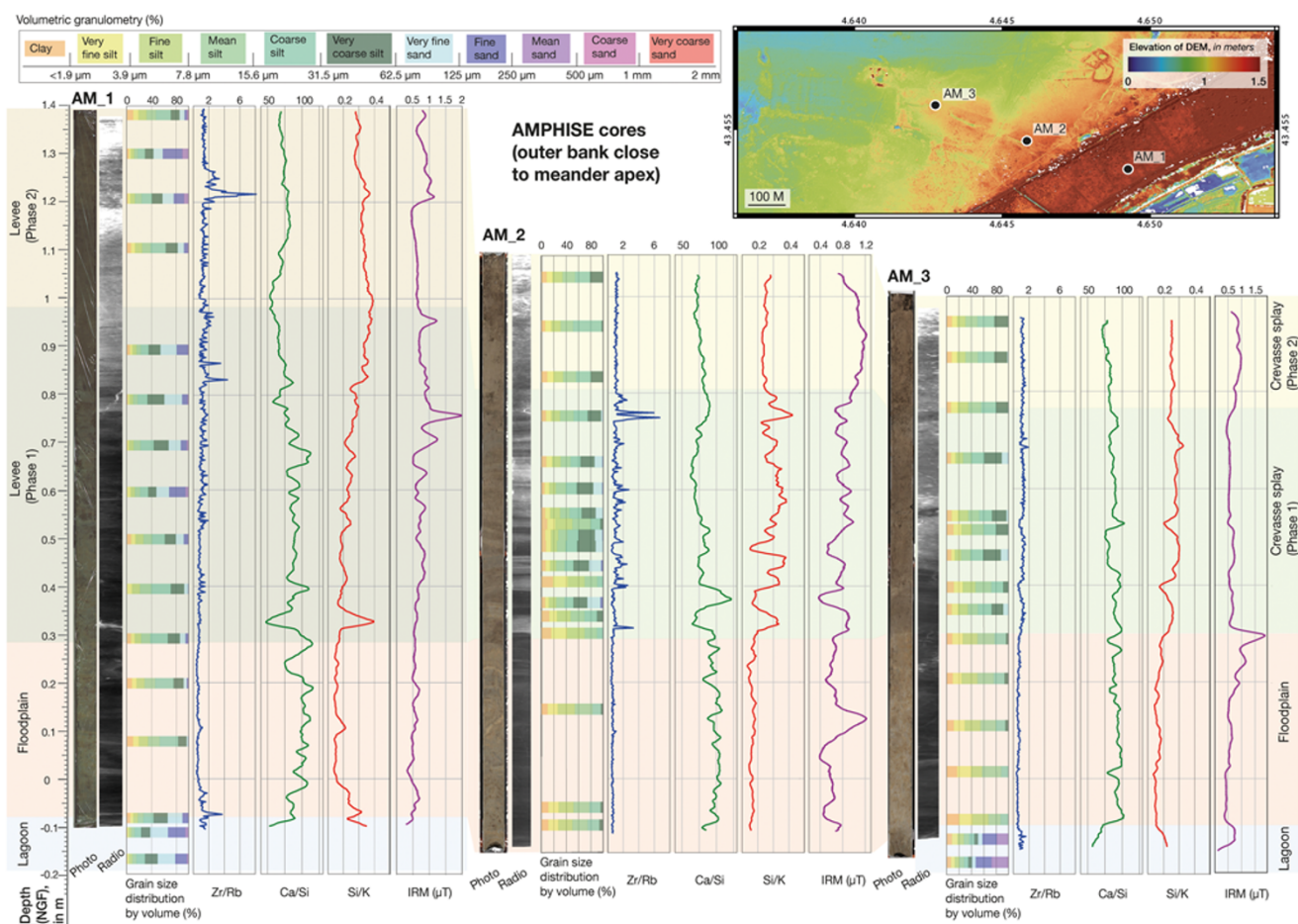
Figure 9. Sediment cores AM_1, AM_2, and AM_3 from overbank deposits at Amphise, with logs showing photographs, radiography, volumetric granulometry, isothermal remanent magnetisation (IRM) magnetic field, and elemental ratios (Zr/Rb, Ca/Si, Si/K). Cores record fluvial environments, with basal floodplain deposits overlain by levee (AM_1) and crevasse splay deposits (AM_2, AM_3). The overbank deposits are subdivided into two depositional phases, distinguishable vertically and laterally relative to the Bras de Fer channel. Additional cores are presented available in Supplementary Material 6. NGF, Nivellement Général de la France (French national vertical datum). (French national vertical datum)

The geometry of the crevasse splays (lobe-shaped, <250 m wide, and <200 m long) and their sedimentary organisation correspond to distributive, non-channelised flow typical of low-gradient floodplains (Coleman, 1969; Gulliford et al., 2017; Millard et al., 2017). The modest extent and silty composition of Grande Ponche crevasse splays reflect the fine sediment input and low-gradient floodplain.

Rapid lateral channel migration, high discharges, and bar instability likely increased overbank flooding and crevasse splay formation (Coleman, 1969). The deposits at Grande Ponche are interpreted as products of these processes. While individual crevasse splays elsewhere may account for 60–70% of overbank stratigraphy (Burns et al., 2017) and form complexes up to 221 km^2 (Rahman et al., 2022), those at Grande Ponche form a stacked succession over ~5 km^2 along a migrating meander.

3. Magnetic and elemental proxies indicating abrupt pulses of detrital sediment input.

Magnetic (IRM) and elemental (Zr/Rb, Ca/Si, Si/K) proxies record discrete pulses of detrital influx linked to flood events. Low IRM values align with coarse-grained overbank deposits, while sustained high IRM intensities correspond to finer-grained, floodplain sedimentation (Fig. 9). Strong magnetic signals occur where coarse diamagnetic quartz is scarce and ferromagnetic minerals, transported within clay fractions, predominate. Conversely, low IRM values and low Si/K ratios indicate dilution by quartz-rich material.

Elevated Zr/Rb and Ca/Si ratios during phase 1 reflect coarse sediments from the Massif Central and Rhône Basin limestone catchments (Arnaud-Fassetta and Provansal, 1999; Stanley and Jorstad, 2002). Their decline in phase 2, alongside rising IRM intensities, marks a transition to finer sedimentation under lower-energy conditions. Zr/Rb ratios peak in AM_1 and AM_2, near the levee breach, reflecting a coarse Zr-bearing sediment input, while AM_3, more distal, records finer-grained material (Fig. 9).

Sedimentary characteristics, such as the absence of bioturbation, the presence of graded bedding, and the geochemical signals (elevated Zr/Rb and Ca/Si in phase 1; high IRM in phase 2), indicate rapid deposition.

The k-means clustering based on elemental ratios and magnetic signatures (Fig. 11) confirms four distinctive facies (floodplain, lagoon, levee, and crevasse splay). Lagoonal facies form a well-defined and distinct cluster, whereas fluvial facies show more overlap. Confusion is frequent between levee and crevasse splay facies (clusters 1 and 3). These overbank deposits are polyphased and share similar compositions. They can include fine silty-clayey laminae deposited during waning flood stages,
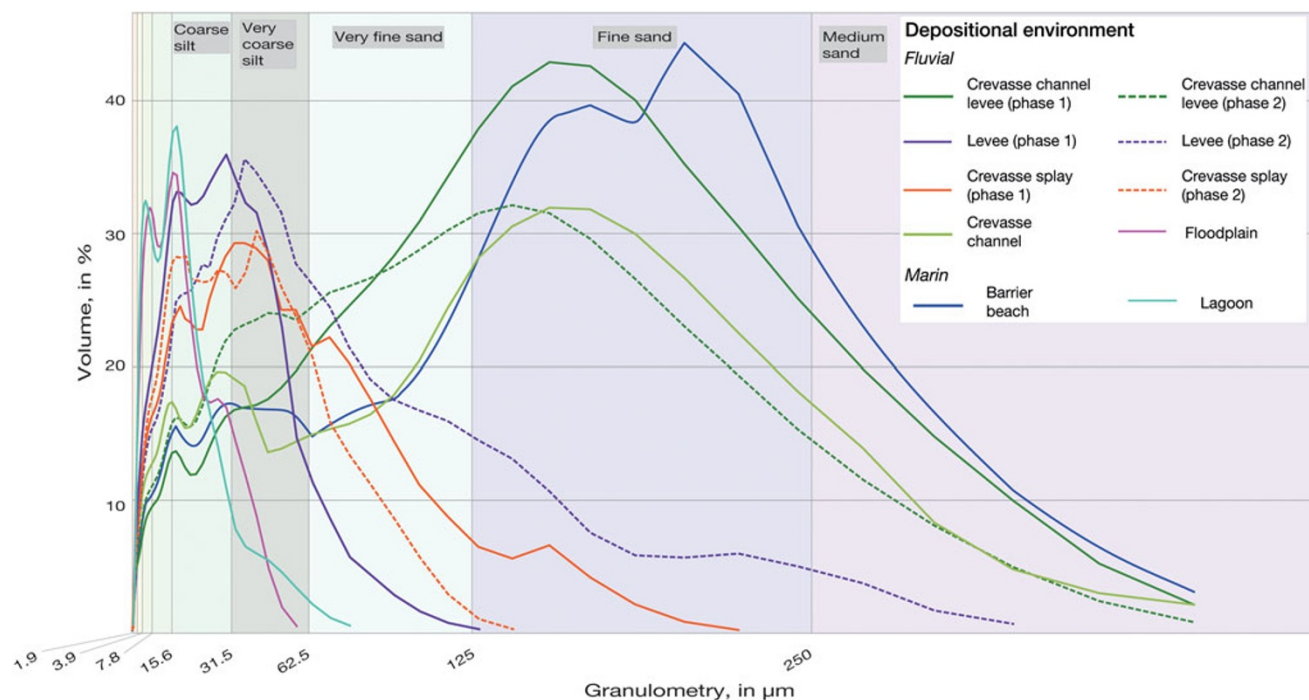
Figure 10. Grain-size distributions (in μm) for fluvial overbank facies of the Grande Ponche and underlying lagoon-marine deposits. Error margins are detailed in Supplementary Material 1.

Figure 11. The k-means classification of sedimentary facies (floodplain, lagoon, levee, and crevasse splay) based on geochemical ratios (Zr/Rb, Ca/Si, Si/K) and isothermal remanent magnetisation (IRM) magnetic field intensity, projected onto the principal component analysis (PCA) PCA plane. This figure presents the classification of U-channel samples collected at 2 mm intervals from overflow deposits in the Grande Ponche area. Symbol shapes indicate facies identified through previous sedimentological analyses. Colours represent four k-means clusters derived from geochemical ratios and IRM intensity: floodplain (cluster 4), lagoon (cluster 2), levee (cluster 1), and crevasse splay (cluster 3). The PCA projection shows that PC1 (x-axis) is driven by Si/K and Zr/Rb ratios, with moderate input from Ca/Si, while PC2 (y-axis) reflects mainly IRM intensity and moderate Ca/Si. The inset correlation circle highlights the geochemical contributions to component separation and facies differentiation.
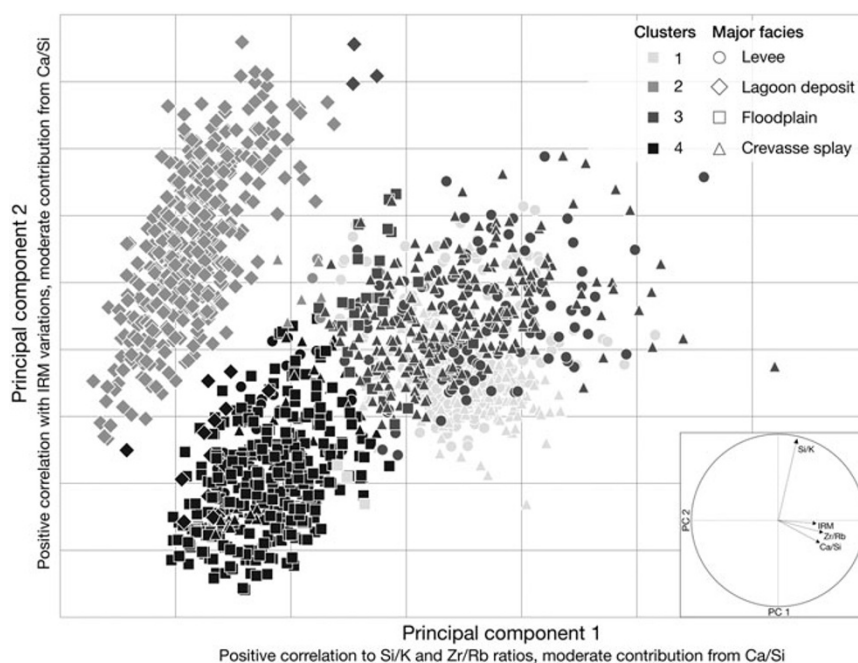
leading to geochemical signatures that partly resemble those of floodplain deposits. Topographic context helps differentiate distal crevasse splays from the higher-elevation levees. Moreover, low IRM values typically align with coarse-grained overbank layers and channel-proximal settings, while consistently elevated IRM intensities characterise fine-grained, magnetically enriched floodplain sediments.

Our findings demonstrate that short-term climatic variability exerted a control on the fluvial dynamics of the Rhône delta during the late LIA, driving rapid meander migration and overbank accretion. The following discussion situates the Grande Ponche case within a broader geomorphological and palaeoclimatic framework, considering the implications for deltaic systems under hydroclimatic forcing.
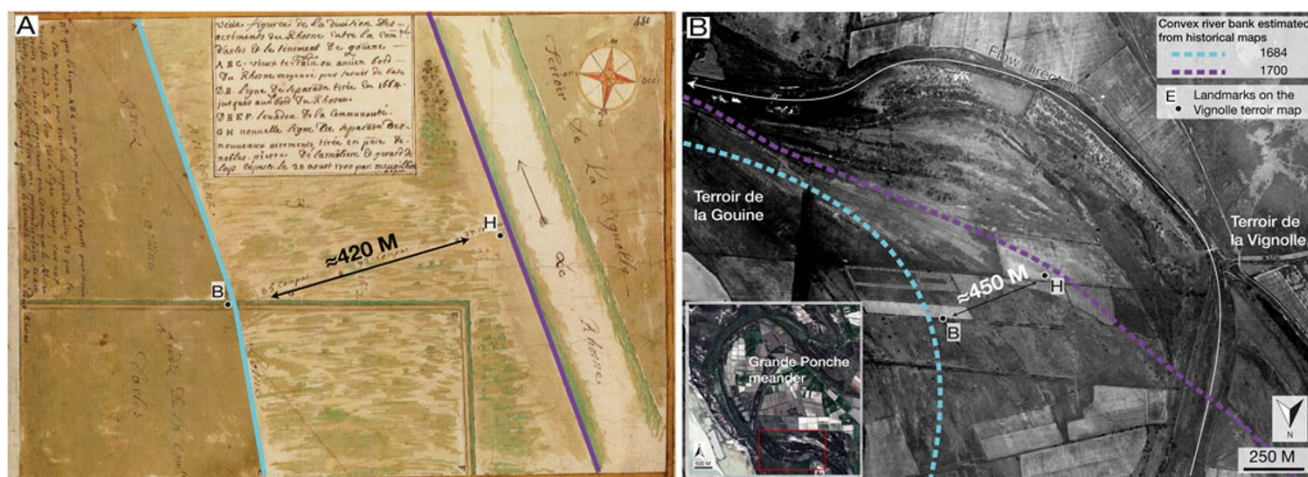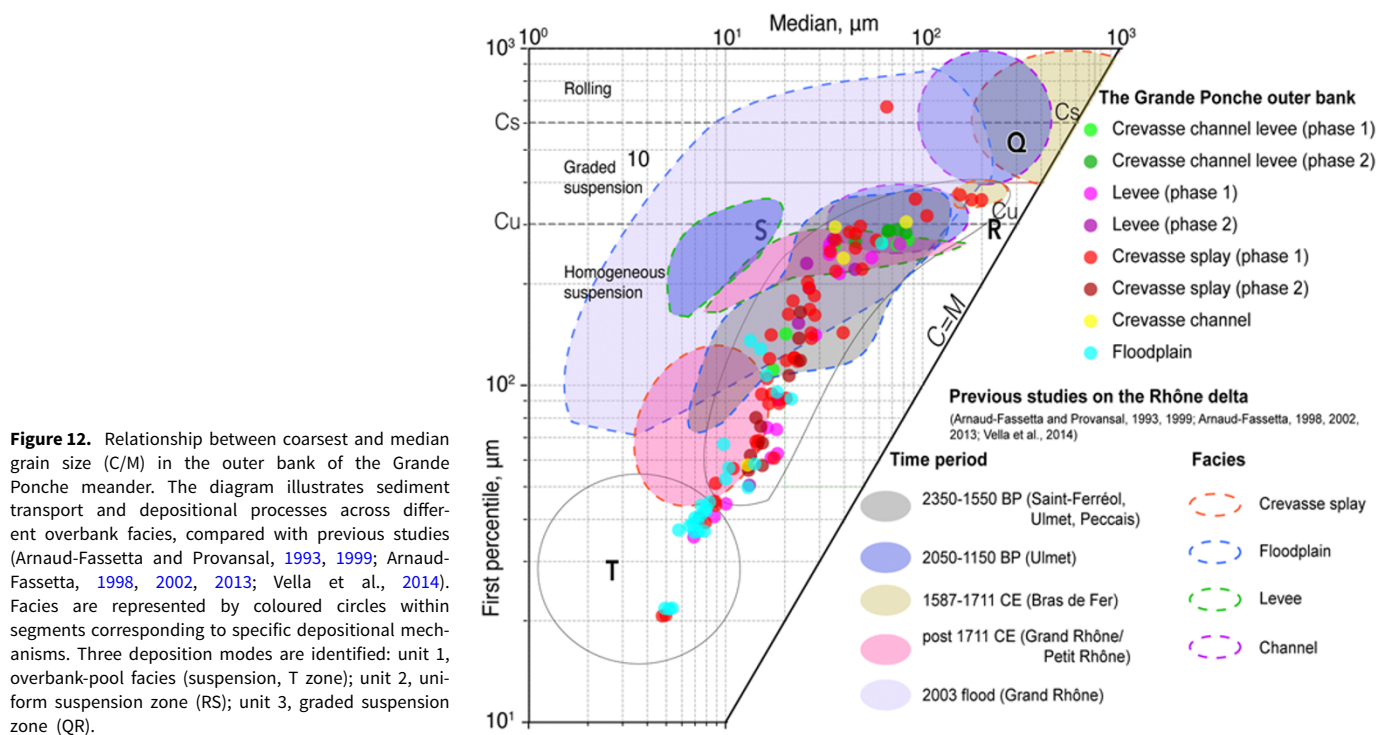
Figure 12. Relationship between coarsest and median grain size (C/M) in the outer bank of the Grande Ponche meander. The diagram illustrates sediment transport and depositional processes across different overbank facies, compared with previous studies (Arnaud-Fassetta and Provansal, 1993, 1999; Arnaud-Fassetta, 1998, 2002, 2013; Vella et al., 2014). Facies are represented by coloured circles within segments corresponding to specific depositional mechanisms. Three deposition modes are identified: unit 1, overbank-pool facies (suspension, T zone); unit 2, uniform suspension zone (RS); unit 3, graded suspension zone (QR).

Figure 13. "Vue figurée de la division des acretements du Rhône entre la comté d'Arles et le tenement de Gouine" (Source: AC Arles - 1Fi282, Arles municipal archives: https://arles.fr/decouvrir/les-archives-communales/consultation-des-archives-communales/). (**A**) Localised map around La Vignolle showing two former Rhône shorelines (1684 and 1700 CE), with an estimated inside bank gain of 215 "compas" (~418 m). (**B**) Image of the area likely corresponding to the tract indicated on the Vignolle map, identified through landscape similarities and distances between former shorelines mapped in 1688 and 1706 (points B and H in A).

Discussion

Climatic forcing and rapid fluvial adjustment

The late LIA evolution of the Grande Ponche meander demonstrates that 1650–1710 CE climatic variability, likely associated with an AMO+ phase, triggered extreme floods and rapid geomorphic adjustments in the Rhône delta. Historical cartography and stratigraphy reveal significant meander migration and widespread crevasse-splay deposition over more than 5 km², reflecting a high sensitivity of deltaic rivers to decadal-scale hydroclimatic forcing.

While a study from the Mississippi suggests stronger flood events during AMO− phases (Munoz et al., 2018), our results highlight a contrasting regional response, where AMO+ appears to coincide with intensified flooding. This emphasises the importance of local climatic–hydrologic coupling in determining fluvial dynamics.

A strengthened summer North Atlantic Oscillation may have further contributed to increased runoff in the Rhône catchment (Schulte et al., 2015).

Sedimentary records of intense flood pulses

The underlying lagoonal sediments, identified at −0.1 m NGF (Nivellement Général de la France, French national vertical datum) at Amphise and between −0.25 and −0.65 m NGF at Pont de l'Aube, are consistent with observations at Saint-Bertrand
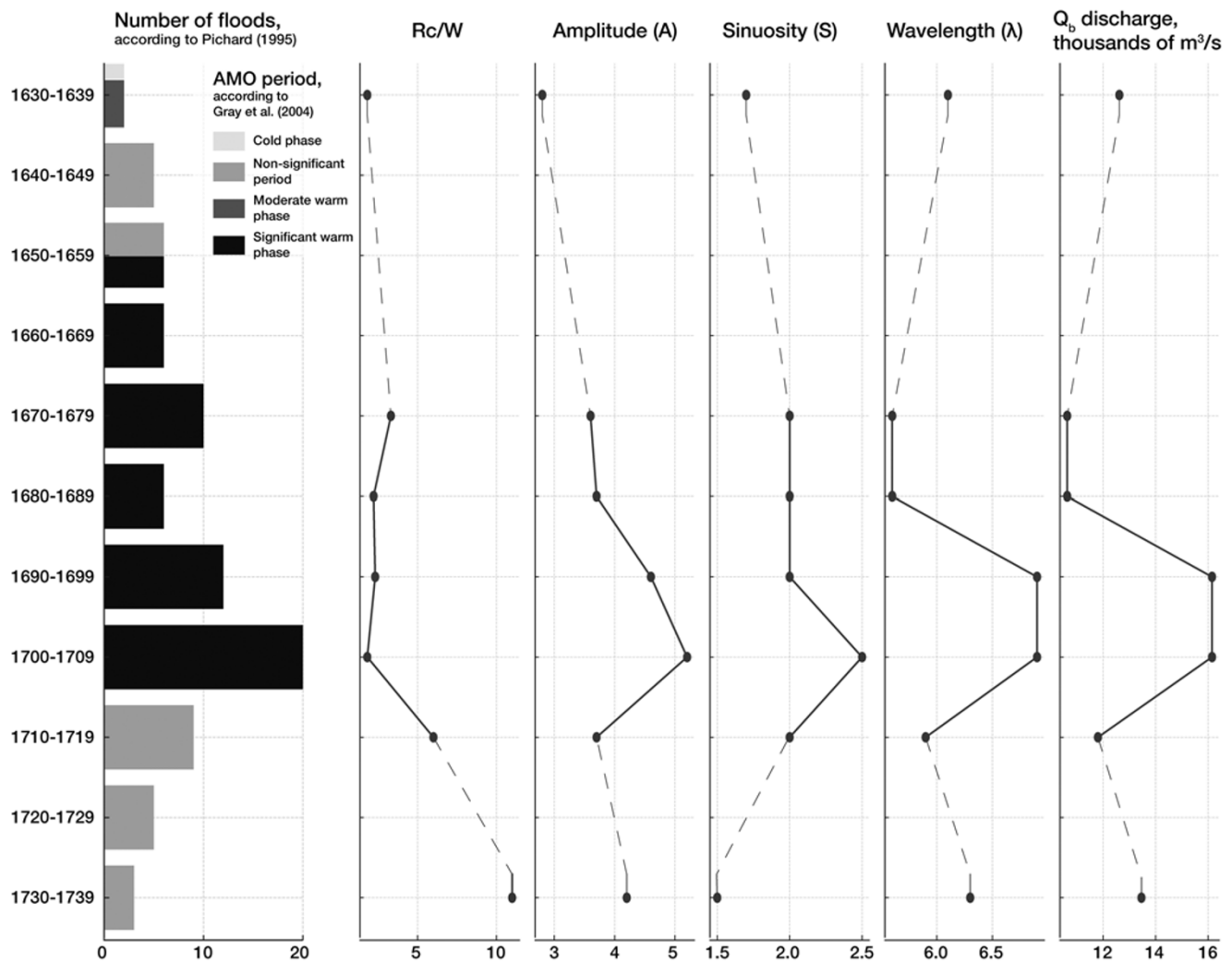
Figure 14. Hydromorphological evolution and flood frequency (Pichard, 1995) of the Grande Ponche meander (1630–1739 CE) in relation to Atlantic Multidecadal Oscillation (AMO) phases (Gray et al., 2004). Flood frequency peaks during AMO+ phases, suggesting a climatic influence. Morphometric parameters (Rc/W declining; amplitude, sinuosity, and wavelength increasing) indicate meander instability and progression towards abandonment. Estimated bankfull discharges (~16,000 m³/s) exceed modern Rhône flood values, reflecting extreme hydrological conditions.

(Arnaud-Fassetta, 1998) and indicate that the present fluvial landscape evolved through the infilling of former coastal environments during delta progradation. The presence of *Cerastoderma edule* and *Bittium reticulatum* further attests to low-energy lagoonal conditions, as similarly recorded near the Ulmet palaeochannel (Vella et al., 2016).

Units on the outside bank (Fig. 15) partially align with channel fill inside bank sequences described by Arnaud-Fassetta (1998). Early deposits (Unit 1) likely record distal events before major accretion (1695–1711 CE). Subsequent phases match Channel Units I–III, suggesting late-stage floods enhanced overbank buildup. Post-1711 avulsion reactivated parts of the channel (Units IV–V) but had limited impact on distal deposits.

The CM diagram (Fig. 12) allows comparison with sediment transport dynamics across the Rhône delta. Unlike the spatial sorting typical of fluvial systems (Passega, 1977), no clear grain-size gradient is observed at the Grande Ponche outer bank. This likely reflects local depositional controls—short transport distances, repeated sediment reworking—and possible sampling limitations.

Similar patterns have been reported elsewhere in the delta, where overbank and channel deposits often plot within the same CM fields, particularly the RS domain, despite granulometric differences (Arnaud-Fassetta, 2002; Vella et al., 2014). This overlap suggests a broad range of flow competence and supports the interpretation of hydrodynamic continuity between channel and overbank processes.

The Grande Ponche sediments are broadly comparable to floodplain deposits dated between 2350 and 1550 BP at Saint-Ferréol, Ulmet, and Peccais (Arnaud-Fassetta, 2002). At Ulmet, levees are finer, while channel fills range from similar to coarser than overbank deposits at Bras de Fer (Arnaud-Fassetta and Provansal, 1993; Vella et al., 2014).

Post-1711 CE crevasse splay and levee deposits in the Grand and Petit Rhône are generally finer (Arnaud-Fassetta and Provansal, 1993), whereas the 2003 flood deposits are as coarse—or coarser (Arnaud-Fassetta, 2013)—than those at Grande Ponche (Fig. 12), indicating high-energy deposition likely linked to artificial levee breaches and concentrated overbank flows.
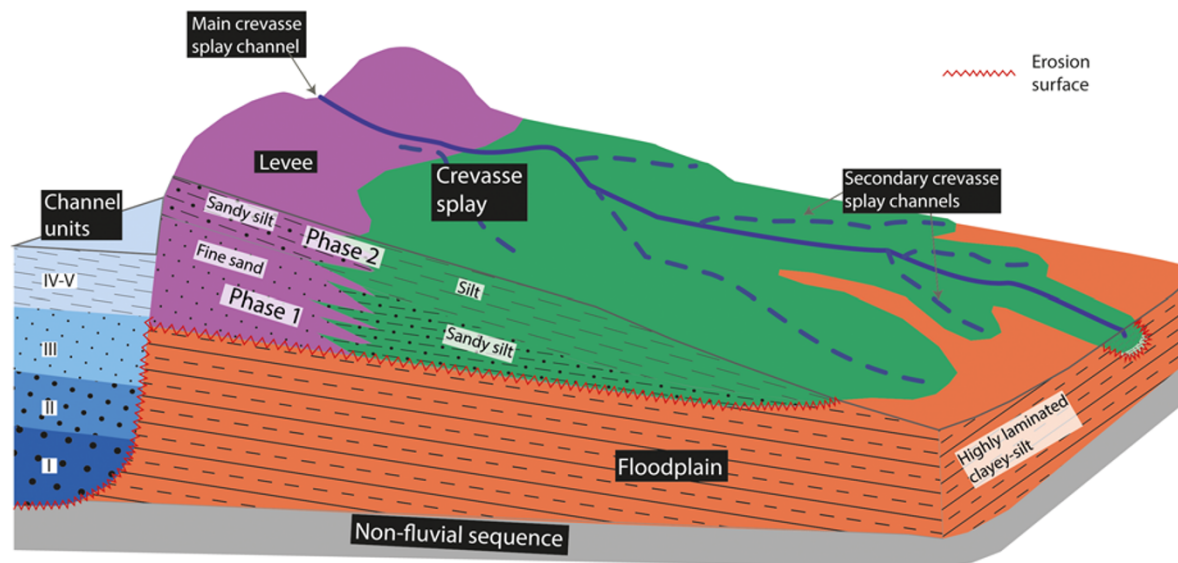
Figure 15. Conceptual diagram of stratigraphy and sediment textures of overbank and channel deposits in the Grande Ponche meander. Overbank units partially correspond to sedimentary core data from palaeochannels documented by Arnaud-Fassetta (1998); The floodplain (overbank unit 1) likely represents distal deposits from older channel systems predating the 1695 CE meander expansion. Cores BF2 and BFII reveal three phases of channel activity: (1) coarse sands from high-energy bars; (2) finer deposits from reduced flow; and (3) moderately coarse, thick sands. These phases correspond to two overbank units: Unit 2 (proximal sandy levee and distal sandy silt crevasse splay) and Unit 3 (proximal sandy silt levee and distal silty crevasse splay).

All Grande Ponche samples were pretreated to remove organic matter and carbonates, ensuring accurate characterisation of the detrital fraction. Earlier studies may not have followed the same protocol, potentially inflating apparent grain sizes. Methodological differences may thus partly explain intersite variability.

The Grande Ponche crevasse splays, despite numerous similarities, exhibit distinct characteristics compared with other examples. Their small size and simple architecture contrast with the complex, amalgamated crevasse splays described by Burns et al. (2017) in Cretaceous systems and by Gulliford et al. (2017) in fine-grained floodplain successions, likely reflecting differences in channel scale, sediment supply, and floodplain accommodation.

Unlike large crevasse splays in broad floodplains (Coleman, 1969; Aslan et al., 2005), the Grande Ponche deposits reflect a confined environment limiting sediment dispersal. The dominance of silt and the scarcity of fine sand, in contrast to coarser examples (O'Brien and Wells, 1986; Millard et al., 2017), highlight the role of local hydrosedimentary conditions.

The persistence and recurrence of crevasse splays at Grande Ponche, unusual in European river systems, point to a strong interplay between LIA climatic forcing and Rhône-specific fluvial dynamics.

Implications for deltaic environments

Holocene sea-level changes in the western Mediterranean were complex, shaped by climatic, isostatic, and tectonic factors (Di Donato et al., 1999; Calafat et al., 2022; Marriner et al., 2023). During the LIA, relative sea-level rise slowed considerably (Vacchi et al., 2018, 2021), allowing riverine sediment inputs to dominate delta dynamics.

These trends were modulated by the AMO and Atlantic Meridional Overturning Circulation, influencing North Atlantic heat transport and Mediterranean levels (Marriner et al., 2023).

Stabilised sea levels during the LIA varied spatially due to atmospheric pressure, sterodynamic effects, and glacial ice loss (Calafat et al., 2022). Prevailing wet conditions contrasted with earlier dry phases (Fletcher and Zielhofer, 2013). Glacio-hydro-isostatic adjustments, enhanced by distance from former ice sheets, also modulated sea levels, particularly in tectonically stable areas like the southern Peloponnese (Lambeck, 1995).

Although marine influence during the LIA was limited, it remains crucial for interpreting delta evolution. The Bras de Fer prograded by ~1.5 km between 1635 and 1678 CE (authors of this study, unpublished data), despite the modest sea-level rise (0.45 ± 0.7 to 0.6 ± 0.6 mm/yr; Vacchi et al., 2021). Simultaneously, the Grande Ponche meander underwent significant vertical aggradation, reflecting enhanced fluvial input and overbank sedimentation.

Recent Mediterranean sea-level rise has accelerated, reaching 3.6 ± 0.4 mm/yr (2000–2018), driven by warming and ice melt (Calafat et al., 2022). Projections estimate a rise to ~4.2 mm/yr by 2040–2050 (Galassi and Spada, 2014), and potentially ~6–10 mm/yr by 2100 under high-emission scenarios (Lionello and Scarascia, 2018). These rates exceed those of the LIA, increasing risks of shoreline retreat and salinisation. Sustained sediment delivery remains essential for delta resilience (Fu et al., 2020; Curtis et al., 2021), partially mitigating sea-level rise impacts.

The Grande Ponche case illustrates fluvial sensitivity to short-term climatic forcing, although extrapolation to other deltas must be cautious. Observed dynamics—meander migration, overbank accretion, crevasse splay formation—reflect local sediment supply, floodplain morphology, and hydroclimate. These processes are not directly applicable to wave- or tide-dominated systems. Broader generalisation requires comparative studies across diverse deltas. This study thus enhances understanding of climate–fluvial interactions in deltaic plains and highlights the need for further research on variability and thresholds across settings.

Conclusion

This study reconstructs the rapid evolution of the Grande Ponche meander during the LIA, illustrating how short-term climatic oscillations influence fluvial dynamics in deltaic settings. Using a multiproxy approach combining historical cartography, topography, sedimentology, geochemistry, and geophysics, we show that episodes of more frequent flooding, associated with positive AMO phases, triggered rapid meander migration and extensive overbank deposition between 1650 and 1710 CE.

Our findings reveal that climatic oscillations promoted hydro-morphological instability, leading to significant sediment redistribution through crevasse splay deposition. Sedimentary, geochemical, and magnetic proxies document abrupt pulses of detrital input by large floods, recording the sensitivity of the Rhône delta to decadal-scale hydroclimatic forcing despite relatively stable sea levels.

The Grande Ponche case study underscores the capacity of deltaic environments to respond to short-term climatic fluctuations. It also illustrates the value of multiproxy approaches for reconstructing past fluvial processes at fine (decadal) temporal and spatial resolution. These findings contribute to a broader understanding of climate–fluvial interactions and offer key insights for predicting the future resilience of deltaic systems in the context of accelerated sea-level rise and anthropogenic pressures.

References

Aloïsi, J.C., 1986. Sur un modèle de sédimentation deltaïque: contribution à la connaissance des marges passives. Doctoral dissertation, Université de Perpignan Via Domitia, Perpignan, France.

Anthony, E.J., Brunier, G., Besset, M., Goichot, M., Dussouillez, P., Nguyen, V.L., 2015. Linking rapid erosion of the Mekong River delta to human activities. *Scientific Reports* **5**, 14745.

Antonelli, C., 2002. Flux sédimentaires et morphogenèse récente dans le chenal du Rhône aval. Doctoral dissertation, Aix-Marseille Université, Aix-en-Provence, France.

Arnaud-Fassetta, G., 1998. Dynamiques fluviales holocènes dans le delta du Rhône. Doctoral dissertation, Aix-Marseille Université, Aix-en-Provence, France.

Arnaud-Fassetta, G., 2000. *Quatre mille ans d'histoire hydrologique dans le delta du Rhône. De l'âge du bronze au siècle du nucléaire*. Grafigéo, 11, Collection mémoires et documents de l'UMR PRODIG, Paris, p. 229.

Arnaud-Fassetta, G., 2002. Geomorphological records of a "flood-dominated regime" in the Rhône Delta (France) between the 1st century BC and the 2nd century AD. What correlations with the catchment paleohydrology?. *Geodinamica Acta* **15**, 79–92.

Arnaud-Fassetta, G., 2003. River channel changes in the Rhone Delta (France) since the end of the Little Ice Age: geomorphological adjustment to hydro-climatic change and natural resource management. *Catena* **51**, 141–172.

Arnaud-Fassetta, G., 2013. Dyke breaching and crevasse-splay sedimentary sequences of the Rhône Delta, France, caused by extreme riverflood of December 2003. *Geografia Fisica e Dinamica Quaternaria* **36**, 7–26.

Arnaud-Fassetta, G., Bruneton, H., Berger, J., Beaudouin, C., Boes, X., Provansal, M., 2005. A ~ 8,000-yr record of palaeohydrology and environmental change in fluvial influenced sediments from Arles-Piton core, upper Rhône Delta, France. *Zeitschrift für Geomorphologie* **49**, 455–484.

Arnaud-Fassetta, G., Provansal, M., 1993. Étude géomorphologique du delta du Rhône: évolution des milieux de sédimentation fluviatiles au cours de l'Holocène récent. *Méditerranée* **78**(3–4), 31–42.

Arnaud-Fassetta, G., Provansal, M., 1999. High frequency variations of water flux and sediment discharge during the Little Ice Age (1586–1725 AD) in the Rhône Delta (Mediterranean France). Relationship to the catchment basin. In: Garnier, J., Mouchel J.-M. (Eds.), *Man and River Systems: The Functioning of River Systems at the Basin Scale*. Developments in Hydrobiology (repr. *Hydrobiologia* **410**, 241–250). Springer, Dordrecht, Netherlands.

Aslan, A., Autin, W.J., Blum, M.D., 2005. Causes of river avulsion: insights from the late Holocene avulsion history of the Mississippi River, USA. *Journal of Sedimentary Research* **75**, 650–664.

Bagnold, R.A., 1960. Some Aspects of the Shape of River Meanders. U.S. Geological Survey Professional Paper 282-E. Washington, DC: Government Printing Office.

Bellmunt, F., Gabas, A., Macau, A., Benjumea, B., Vilà, M., Figueras, S., 2022. Sediment characterization in deltas using electrical resistivity tomography: the Ebro delta case. *Journal of Applied Geophysics* **196**, 104520.

Bellotti, P., Caputo, C., Davoli, L., Evangelista, S., Garzanti, E., Pugliese, F., Valeri, P., 2004. Morpho-sedimentary characteristics and Holocene evolution of the emergent part of the Ombrone River delta (southern Tuscany). *Geomorphology* **61**, 71–90.

Besset, M., Anthony, E.J., Sabatier, F., 2017. River delta shoreline reworking and erosion in the Mediterranean and Black Seas: the potential roles of fluvial sediment starvation and other factors. *Elementa: Science of the Anthropocene* **5**, 54.

Bhattacharya, J.P., Giosan, L., 2003. Wave-influenced deltas: geomorphological implications for facies reconstruction. *Sedimentology* **50**, 187–210.

Blott, S.J., Pye, K., 2012. Particle size scales and classification of sediment types based on particle size distributions: review and recommended procedures. *Sedimentology* **59**, 2071–2096.

Bond, G., Kromer, B., Beer, J., Muscheler, R., Evans, M. N., Showers, W., Hoffmann, S., Lotti-Bond, R., Hajdas, I., Bonani, G., 2001. Persistent solar influence on North Atlantic climate during the Holocene. *Science* **294**, 2130–2136.

Boudet, L., Sabatier, F., Radakovitch, O., 2017. Modelling of sediment transport pattern in the mouth of the Rhone delta: role of storm and flood events. *Estuarine, Coastal and Shelf Science* **198**, 568–582.

Boyd, R., Dalrymple, R., Zaitlin, B.A., 1992. Classification of clastic coastal depositional environments. *Sedimentary Geology* **80**(3–4), 139–150.

Bravard, J.P., 1989. La métamorphose des rivières des Alpes françaises à la fin du Moyen Âge et à l'époque moderne. *Bulletin de la Société géographique de Liège* **25**, 145–157.

Bravard, J.P., 2010. Discontinuities in braided patterns: the River Rhône from Geneva to the Camargue delta before river training. *Geomorphology* **117**, 219–233.

Bravard, J.P., Goichot, M., Tronchère, H., 2014. An assessment of sediment-transport processes in the Lower Mekong River based on deposit grain sizes, the CM technique and flow-energy data. *Geomorphology* **207**, 174–189.

Bravard, J.P., Lippmann-Provansal, M., Arnaud-Fassetta, G., Chabbert, S., Gaydou, P., Dufour, S., Richard, F., Valleteau, S., Melun, G., Passy, P., 2008. Un atlas du paléo-environnement de la plaine alluviale du Rhône, de la frontière suisse à la mer. Collection EDYTEM. *Cahiers de géographie* **6**, 101–116.

Bridge, J.S., 2006. Fluvial facies models: recent developments.In: Posamentier, H., Walker, R.G. (Eds.), *Facies Models Revisited*. SEPM Special Publication, no. 84. SEPM (Society for Sedimentary Geology), Tulsa, OK, pp. 85–170.

Broecker, W.S., 2000. Was a change in thermohaline circulation responsible for the Little Ice Age? *Proceedings of the National Academy of Sciences USA* **97**, 1339–1342.

Brönnimann, S., Franke, J., Nussbaumer, S.U., Zumbühl, H.J., Steiner, D., Trachsel, M., Hegerl, G.C., *et al.*, 2019. Last phase of the Little Ice Age forced by volcanic eruptions. *Nature Geoscience* **12**, 650–656.

Burns, C.E., Mountney, N.P., Hodgson, D.M., Colombera, L., 2017. Anatomy and dimensions of fluvial crevasse-splay deposits: examples from the Cretaceous Castlegate Sandstone and Neslen Formation, Utah, USA. *Sedimentary Geology* **351**, 21–35.

Calafat, F.M., Frederikse, T., Horsburgh, K., 2022. The sources of sea-level changes in the Mediterranean Sea since 1960. *Journal of Geophysical Research: Oceans* **127**, e2022JC019061.

Caritey, C., 1995. *L'évolution de l'embouchure du Rhône du milieu du XVIIe à la fin du XIXe siècle*. Mémoire de Maîtrise. Aix-Marseille Université, Aix-en-Provence, France.

Carozza, J.M., Puig, C., Odiot, T., Valette, P., Passarrius, O., 2012. Lower Mediterranean plain accelerated evolution during the Little Ice Age: geoarchaeological insight in the Tech basin (Roussillon, Gulf of Lion, Western Mediterranean). *Quaternary International* **266**, 94–104.

Clayton, J.A., Pitlick, J., 2007. Spatial and temporal variations in bed load transport intensity in a gravel bed river bend. *Water Resources Research* **43**(2), W02426.

Clift, P.D., Jonell, T.N., 2021. Monsoon controls on sediment generation and transport: mass budget and provenance constraints from the Indus River catchment, delta and submarine fan over tectonic and multimillennial timescales. *Earth-Science Reviews* **220**, 103682.

[CNES] Centre national d'études spatiales, 2023. Pléiades. https://cnes.fr/projets/pleiades.

Colella, A., 1988. Pliocene-Holocene fan deltas and braid deltas in the Crati Basin, Southern Italy: a consequence of varying tectonic conditions. In: Nemec, W. (Ed.), *Fan Deltas: Sedimentology and Tectonic Settings*. Blackie Academic & Professional, Glasgow, UK, pp. 50–74.

Coleman, J.M., 1969. Brahmaputra River: channel processes and sedimentation. *Sedimentary Geology* **3**, 129–239.

Croudace, I.W., Rindby, A., Rothwell, R.G. 2006. ITRAX: description and evaluation of a new multi-function X-ray core scanner.In: Rothwell, R.G. (Ed.), *New Techniques in Sediment Core Analysis. Geological Society of London Special Publication* **267**, 51–63.

Curtis, J.A., Flint, L.E., Stern, M.A., Lewis, J., Klein, R.D., 2021. Amplified impact of climate change on fine-sediment delivery to a subsiding coast, Humboldt Bay, California. *Estuaries and Coasts* **44**, 2173–2193.

Curtis, S., 2008. The Atlantic multidecadal oscillation and extreme daily precipitation over the US and Mexico during the hurricane season. *Climate Dynamics* **30**, 343–351.

Dalrymple, R.W., Zaitlin, B.A., Boyd, R., 1992. Estuarine facies models; conceptual basis and stratigraphic implications. *Journal of Sedimentary Research* **62**, 1130–1146.

Demory, F., Uehara, M., Quesnel, Y., Rochette, P., Romey, C., Tachikawa, K., Escutia, C., *et al*., 2019. A new high-resolution magnetic scanner for sedimentary sections. *Geochemistry, Geophysics, Geosystems* **20**, 3186–3200.

Di Donato, G., Negredo, A.M., Sabadini, R., Vermeersen, L.L.A., 1999. Multiple processes causing sea-level rise in the central Mediterranean. *Geophysical Research Letters* **26**, 1769–1772.

Duboul-Razavet, C., Duplaix, S., 1956. Contribution à l'étude géologique et sédimentologique du delta du Rhône: par Christiane Duboul-Razavet. Étude pétrographique des formations meubles de la Gascogne du pays basque et de leur littoral. *Mémoires de la Société géologique de France, nouvelle série* **35**(3–4), 234–108. Société géologique de France, Paris.

Dury, G.H., 1955. Bed-width and wave-length in meandering valleys. *Nature* **176**, 31–32.

Dury, G.H., 1976. Discharge prediction, present and former, from channel dimensions. *Journal of Hydrology* **30**, 219–245.

Ericson, J.P., Vörösmarty, C.J., Dingman, S.L., Ward, L.G., Meybeck, M., 2006. Effective sea-level rise and deltas: causes of change and human dimension implications. *Global and Planetary Change* **50**(1–2), 63–82.

Fanget, A.S., Berné, S., Jouet, G., Bassetti, M.A., Dennielou, B., Maillet, G.M., Tondut, M., 2014. Impact of relative sea level and rapid climate changes on the architecture and lithofacies of the Holocene Rhone subaqueous delta (Western Mediterranean Sea. *Sedimentary Geology* **305**, 35–53.

Filgueira-Rivera, M., Smith, N.D., Slingerland, R.L., 2007. Controls on natural levee development in the Columbia River, British Columbia, Canada. *Sedimentology* **54**, 905–919.

Fletcher, W.J., Zielhofer, C., 2013. Fragility of Western Mediterranean landscapes during Holocene rapid climate changes. *Catena* **103**, 16–29.

Florsch, N., Muhlach, F., 2018. *Géophysique appliquée pour tous 1: Méthodes électriques*. Vol. 1. ISTE Group, London.

Fu, S., Xiong, H., Zong, Y., Huang, G., 2020. Reasons for the low sedimentation and slow progradation in the Pearl River delta, southern China, during the middle Holocene. *Marine Geology* **423**, 106133.

Galassi, G., Spada, G., 2014. Sea-level rise in the Mediterranean Sea by 2050: roles of terrestrial ice melt, steric effects and glacial isostatic adjustment. *Global and Planetary Change* **123**, 55–66.

Galloway, W.E., 1975. *Process Framework for Describing the Morphologic and Stratigraphic Evolution of Deltaic Depositional Systems*. SEPM Special Publication, no. 31. SEPM (Society for Sedimentary Geology), Tulsa, OK, 127–156.

Goodbred, S.L. Jr, 2003. Response of the Ganges dispersal system to climate change: a source-to-sink view since the last interstade. *Sedimentary Geology* **162**(1–2), 83–104.

Gray, S.T., Graumlich, L.J., Betancourt, J.L., Pederson, G.T., 2004. A tree-ring based reconstruction of the Atlantic Multidecadal Oscillation since 1567 AD. *Geophysical Research Letters* **31**(12), L12205.

Gulliford, A.R., Flint, S.S., Hodgson, D.M., 2017. Crevasse splay processes and deposits in an ancient distributive fluvial system: the lower Beaufort Group, South Africa. *Sedimentary Geology* **358**, 1–18.

Hartigan, J.A. Wong, M.A., 1979. A k–means clustering algorithm. *Applied Statistics* **28**, 100–108.

Hemery, G., 2014. *Les Noms de lieux en Camargue: Toponymie*. Éditions Sansouire, Nîmes.

Hey, R., 1984. Plan geometry of river meanders. In: *River Meandering*. American Society of Civil Engineers (ASCE), New York, pp. 30–43.

Hooke, J.M., 1984. Changes in river meanders: a review of techniques and results of analyses. *Progress in Physical Geography* **8**, 473–508.

Hooke, J.M., 1997. Styles of channel change. In: *Applied Fluvial Geomorphology for River Engineering and Management*. Wiley, Chichester, UK, pp. 237–268.

Hooke, J.M., 2013. River meandering. In: Shroder, J.F. (Ed.), *Treatise on Geomorphology*. Fluvial Geomorphology Vol. 9. Academic Press, San Diego, CA, pp. 260–288.

Hydro.eaufrance, n.d. Station hydrométrique–V720 0010 01: Le Rhône à Tarascon–CNR–Statistiques. SCHAPI–HydroPortail. https://www.hydro.eaufrance.fr/stationhydro/V720001001/qj_annual/statistique/resultat.

[IGN] Institut National de l'Information Géographique et Forestière, 1942. Remonter le temps: Images aériennes de 1942. IGN, Saint-Mandé, France. https://remonterletemps.ign.fr.

[IGN] Institut National de l'Information Géographique et Forestière, 2018. RGE ALTI˚, Version 2.0. Descriptif de contenu. IGN, Saint-Mandé, France. https://geoservices.ign.fr/sites/default/files/2021-07/DC_RGEALTI_2-0.pdf.

[IGN] Institut National de l'Information Géographique et Forestière, 2022. LIDAR HD, Version 1.0. Descriptif technique. IGN, Saint-Mandé, France. https://geoservices.ign.fr/sites/default/files/2022-05/DT_LiDAR_HD_1-0.pdf.

Jolliffe, I.T., Cadima, J., 2016. Principal component analysis: a review and recent developments. *Philosophical Transactions of the Royal Society A* **374**, 20150202.

Keesstra, S.D., Van Huissteden, J., Vandenberghe, J., Van Dam, O., De Gier, J., Pleizier, I.D., 2005. Evolution of the morphology of the river Dragonja (SW Slovenia) due to land-use changes. *Geomorphology* **69**(1–4), 191–207.

Knighton, D., 1998. *Fluvial Forms and Processes: A New Perspective*. Routledge, London.

Knudsen, M.F., Jacobsen, B.H., Seidenkrantz, M.S., Olsen, J., 2014. Evidence for external forcing of the Atlantic Multidecadal Oscillation since termination of the Little Ice Age. *Nature Communications* **5**, 3323.

Laigre, L., Reynard, E., Arnaud-Fassetta, G., Baron, L., Glenz, D., 2012. Caractérisation de la paléodynamique du Rhône en Valais central (Suisse) à l'aide de la tomographie de résistivité électrique. *Géomorphologie: Relief, Processus, Environnement* **18**, 405–426.

Lambeck, K., 1995. Late Pleistocene and Holocene sea-level change in Greece and south-western Turkey: a separation of eustatic, isostatic and tectonic contributions. *Geophysical Journal International* **122**, 1022–1044.

Ladurie, E.L.R., 1967. *Histoire du climat depuis l'an mil*. Vol. 28. Paris, Flammarion.

Landuré, C. & Pasqualini, M., 2004. *Delta du Rhône: Camargue antique, médiévale et moderne. Bulletin Archéologique de Provence*, supplément 2. Aix-en-Provence, France: Association Provence Archéologie, 334 pp.

Leopold, L.B., Wolman, M.G., 1970. River channel patterns. *Rivers and River Terraces*. Palgrave Macmillan UK, London, pp. 197–237.

Lepage, H., Masson, M., Delanghe, D., Le Bescond, C., 2019. Grain size analyzers: results of an intercomparison study. *SN Applied Sciences* **1**, 1–14.

Leveau, P., 2014. Le Rhône romain dans sa basse plaine et dans son delta. Variations territoriales, sociétales et environnementales. *Revue archéologique de Narbonnaise* **47**, 9–34.

Levraut, A.M., Roy, A., 2007. La situation de 1856 est-elle reproductible? Illustration pour le Rhône aval à partir de l'expérience de la crue de décembre 2003. *La Houille Blanche* **93**, 52–55.

L'Homer, A., 1975. Notice explicative de la carte géologique des Saintes-Mariés-de-la-mer au 1/50000, Feuille 1018. Carte géologique de la France à 1/50 000. Bureau de Recherches Géologiques et Minières (BRGM), Orléans, France.

L'Homer, A., Bazile, F., Thommeret, J., Thommeret, Y., 1981. Principales étapes de l'édification du delta du Rhone de 7000 BP à nos jours, variations du niveau marin. *Oceanis* **7**, 389–408.

Lionello, P., Scarascia, L., 2018. The relation between climate change in the Mediterranean region and global warming. *Regional Environmental Change* **18**, 1481–1493.

Maillet, G., 2005. Relations sédimentaires récentes et actuelles entre un fleuve et son delta en milieu microtidal: exemple de l'embouchure du Rhône. Doctoral dissertation, Université de Provence-Aix-Marseille I.

Maillet, G.M., Rizzo, E., Revil, A., Vella, C., 2005. High resolution electrical resistivity tomography (ERT) in a transition zone environment: application for detailed internal architecture and infilling processes study of a Rhône River paleo-channel. *Marine Geophysical Researche* **26**, 317–328.

Maillet, G.M., Vella, C., Provansal, M., Sabatier, F., 2006. Connexions entre le Rhône et son delta (partie 2): évolution du trait de côte du delta du Rhône depuis le début du XVIIIe siècle. *Géomorphologie: relief, processus, environnement* **12**, 125–140.

Mann, M.E., Zhang, Z., Rutherford, S., Bradley, R.S., Hughes, M.K., Shindell, D., Ammann, C., *et al*., 2009. Global signatures and dynamical origins of the Little Ice Age and Medieval Climate Anomaly. *Science* **326**, 1256–1260.

Marriner, N., Kaniewski, D., Morhange, C., Vacchi, M., Kallel, N., Rossignol, I., Cazenave, A., *et al*., 2023. Forecasted weakening of Atlantic overturning circulation could amplify future relative sea–level rise in the Mediterranean: a review of climate and tide–gauge data links. *Earth–Science Reviews* **242**, 104456.

Martinez, T., Deschamps, R., Amorosi, A., Jouet, G., Vella, C., Ducret, G., Berger, J.F., 2024. Holocene stratigraphic architecture of a Mediterranean delta and implication for sediment budget evolution: example of the Rhône delta. *Sedimentary Geology* **462**, 106574.

Millard, C., Hajek, E., Edmonds, D.A., 2017. Evaluating controls on crevasse-splay size: implications for floodplain-basin filling. *Journal of Sedimentary Research* **87**, 722–739.

Miller, G.H., Geirsdóttir, Á., Zhong, Y., Larsen, D.J., Otto-Bliesner, B.L., Holland, M.M., Bailey, D.A., *et al*., 2012. Abrupt onset of the Little Ice Age triggered by volcanism and sustained by sea-ice/ocean feedbacks. *Geophysical Research Letters* **39**(2), L02708.

Munoz, S.E., Giosan, L., Therrell, M.D., Remo, J.W., Shen, Z., Sullivan, R.M., Wiman, C., *et al*., 2018. Climatic control of Mississippi River flood hazard amplified by river engineering. *Nature* **556**, 95–98.

O'Brien, P.E., Wells, A.T., 1986. A small, alluvial crevasse splay. *Journal of Sedimentary Research* **56**, 876–879.

O'Reilly, C.H., Woollings, T., Zanna, L., 2017. The dynamical influence of the Atlantic multidecadal oscillation on continental climate. *Journal of Climate* **30**, 7213–7230.

Owens, M.J., Lockwood, M., Hawkins, E., Usoskin, I., Jones, G.S., Barnard, L., Scott, C.J., *et al*., 2017. The Maunder minimum and the Little Ice Age: an update from recent reconstructions and climate simulations. *Journal of Space Weather and Space Climate* **7**, A33.

Passega, R., 1957. Texture as characteristic of clastic deposition. *AAPG Bulletin* **41**, 1952–1984.

Passega, R., 1964. Grain size representation by CM patterns as a geologic tool. *Journal of Sedimentary Research* **34**, 830–847.

Passega, R., 1977. Significance of CM diagrams of sediments deposited by suspensions. *Sedimentology* **24**, 723–733.

Perșoiu, I., Perșoiu, A., 2019. Flood events in Transylvania during the medieval warm period and the little ice age. *The Holocene* **29**, 85–96.

Pichard, G., 1995. Les crues sur le bas Rhône de 1500 à nos jours. Pour une histoire hydro-climatique. *Méditerranée* **82**, 105–116.

Pichard, G., Provansal, M., Sabatier, F., 2014. Les embouchures du Rhône. L'apport de la cartographie à l'étude de leur évolution géomorphologique au cours du Petit âge glaciaire (PAG). *Méditerranée*, no. 122, 43–59.

Pichard, G., Roucaute, É., 2014. Pluies et crues en bas Rhône et caractérisation du petit âge de glace (PAG). *Méditerranée*, no. 122, 31–42.

Provansal, M., Arnaud-Fassetta, G., Vella, C., 2004. Géomorphologie du delta du Rhône. In C. Landuré & M. Pasqualini (Eds.), *Delta du Rhône: Camargue antique, médiévale et moderne* (*Bulletin Archéologique de Provence*, Supplément 2, pp. 59–63). Aix-en-Provence, France: Éditions de l'Association Provence Archéologie (APA).

Rahman, M.M., Howell, J.A., MacDonald, D.I., 2022. Quantitative analysis of crevasse-splay systems from modern fluvial settings. *Journal of Sedimentary Research* **92**, 751–774.

Reimer, P.J., Austin, W.E., Bard, E., Bayliss, A., Blackwell, P.G., Ramsey, C.B., van der Plicht, J., *et al*., 2020. The IntCal20 Northern Hemisphere radiocarbon age calibration curve (0–55 cal kBP). *Radiocarbon* **62**, 725–757.

Rey, T., Lefèvre, D., Vella, C., 2005. Données nouvelles sur les lobes deltaïques du paléogolfe d'Aigues–Mortes à l'Holocène (Petite Camargue, France). *Quaternaire* **16**, 329–338.

Rey, T., Lefevre, D., Vella, C., 2009. Deltaic plain development and environmental changes in the Petite Camargue, Rhone Delta, France, in the past 2000 years. *Quaternary Research* **71**, 284–294.

Rhoades, J.D., Manteghi, N.A., Shouse, P.J., Alves, W.J., 1989. Estimating soil salinity from saturated soil-paste electrical conductivity. *Soil Science Society of America Journal* **53**, 428–433.

Rossiaud, J., 1994. Réalités et imaginaire d'un fleuve: recherches sur le Rhône médiéval. Doctoral dissertation, Université Paris 1 Panthéon-Sorbonne, Paris.

Ruiz-Pérez, J.M., Carmona, P., 2019. Turia river delta and coastal barrier-lagoon of Valencia (Mediterranean coast of Spain): geomorphological processes and global climate fluctuations since Iberian-Roman times. *Quaternary Science Reviews* **219**, 84–101.

Russell, R.J., 1954. Alluvial morphology of Anatolian rivers. *Annals of the Association of American Geographers* **44**, 363–391.

Sabatier, F., 2001. Fonctionnement et dynamiques morpho-sédimentaires du littoral du delta du Rhône. Doctoral dissertation, Aix-Marseille 3.

Sabatier, F., Anthony, E., 2015. The sand spits of the Rhone River delta: formation, dynamics, sediment budgets and management. In: Randazzo, G., Jackson, D., Cooper, J. (Eds.), *Sand and Gravel Spits*. Coastal Research Library, Vol 12. Springer, Cham, Switzerland, pp. 259–274.

Salomon, F., Keay, S., Strutt, K.D., Goiran, J.P., Millett, M.J., Germoni, P., 2016. Connecting Portus with Ostia: preliminary results of a geoarchaeological study of the navigable canal on the Isola Sacra. *Revue archéologique de Narbonnaise* **44**(Supplément 44), 293–303.

Scheidt, S., Egli, R., Frederichs, T., Hambach, U., Rolf, C., 2017. A mineral magnetic characterization of the Plio-Pleistocene fluvial infill of the Heidelberg Basin (Germany). *Geophysical Journal International* **210**, 743–764.

Schulte, L., Peña, J. C., Carvalho, F., Schmidt, T., Julià, R., Llorca, J., Veit, H., 2015. A 2600-year history of floods in the Bernese Alps, Switzerland: frequencies, mechanisms and climate forcing. *Hydrology and Earth System Sciences* **19**, 3047–3072.

Schumm, S.A., 1981. Evolution and response of the fluvial system, sedimentologic implications. In: Ethridge, F.G., Flores, R.M. (Eds.), *Recent and Ancient Nonmarine Depositional Environments: Models for Exploration*. SEPM Special Publication, no. 31. SEPM (Society for Sedimentary Geology), Tulsa, OK, pp. 19–29.

Schumm, S.A., 1985. Patterns of alluvial rivers. *Annual Review of Earth and Planetary Sciences* **13**, 5–27.

Sclafert, T., 1959. *Cultures en Haute-Provence: déboisements et pâturages au Moyen Âge*. Éditions de l'EHESS, Paris.

Seltzer, G.O., Rodbell, D.T., 2005. Delta progradation and Neoglaciation, Laguna Parón, Cordillera Blanca, Peru. *Journal of Quaternary Science* **20**, 715–722.

Sharifi, A., Murphy, L.N., Pourmand, A., Clement, A.C., Canuel, E.A., Naderi Beni, A., Lahijani, H.A.K., *et al*, 2018. Early-Holocene greening of the Afro-Asian dust belt changed sources of mineral dust in West Asia. *Earth and Planetary Science Letters* **481**, 30–40.

SHOM, 2015. Litto3D°–Descriptif du contenu. Service hydrographique et océanographique de la marine (SHOM), Brest, France. services.data.shom.fr/static/specifications/DC_Litto3D.pdf

Slingerland, R., Smith, N.D., 1998. Necessary conditions for a meandering-river avulsion. *Geology* **26**, 435–438.

Smith, N.D., Cross, T.A., Dufficy, J.P., Clough, S.R., 1989. Anatomy of an avulsion. *Sedimentology* **36**, 1–23.

Stanford, J.D., Hemingway, R., Rohling, E.J., Challenor, P.G., Medina-Elizalde, M., Lester, A.J., 2011. Sea-level probability for the last deglaciation: a statistical analysis of far-field records. *Global and Planetary Change* **79**, 193–203.

Stanley, J.D., Jorstad, T.F., 2002. Iron-coated quartz as a provenance and paleoclimatic marker in the Rhône Delta, France. *Journal of Coastal Research* **18**, 712–729.

Stanley, D.J., Warne, A.G., 1994. Worldwide initiation of Holocene marine deltas by deceleration of sea-level rise. *Science* **265**, 228–231.

Suanez, S. S., Bruzzi, C., Arnoux-Chiavassa, S., 1998. Données récentes sur l'évolution des fonds marins dans le secteur oriental du delta du Rhône (plage Napoléon et flèche de la Gracieuse). *Géomorphologie: Relief, Processus, Environnement* **4**, 291–311.

Syvitski, J.P., Saito, Y., 2007. Morphodynamics of deltas under the influence of humans. *Global and Planetary Change* **57**, 261–282.

Talská, R., Hron, K., Grygar, T.M., 2021. Compositional scalar-on-function regression with application to sediment particle size distributions. *Mathematical Geosciences* **53**, 1667–1695.

Turner, J.N., Jones, A.F., Brewer, P.A., Macklin, M.G., Rassner, S.M., 2015. Micro-XRF applications in fluvial sedimentary environments of Britain and Ireland: progress and prospects. *Micro-XRF Studies of Sediment Cores: Applications of a Non-destructive Tool for the Environmental Sciences*. Developments in Paleoenvironmental Research 17. Springer, Dordrecht, Netherlands, pp. 227–265.

Vacchi, M., Ghilardi, M., Melis, R.T., Spada, G., Giaime, M., Marriner, N., Lorscheid T., *et al*., 2018. New relative sea-level insights into the isostatic history of the Western Mediterranean. *Quaternary Science Reviews* **201**, 396–408.

Vacchi, M., Joyse, K.M., Kopp, R.E., Marriner, N., Kaniewski, D., Rovere, A., 2021. Climate pacing of millennial sea-level change variability in the central and western Mediterranean. *Nature Communications* **12**, 4013.

Vella, C., Fleury, T.J., Gensous, B., Labaune, C., Tesson, M., 2008. Grandes séquences holocènes et discontinuités sédimentaires dans le delta du Rhône. Collection EDYTEM. *Cahiers de géographie* **6**, 155–166.

Vella, C., Fleury, T.J., Raccasi, G., Provansal, M., Sabatier, F., Bourcier, M., 2005. Evolution of the Rhône delta plain in the Holocene. *Marine Geology* **222**, 235–265.

Vella, C., Landuré, C., Long, L., Dussouillez, P., Fleury, J., Tomatis, C., Sivan, O., *et al*., 2016. Ports fluviaux, ports lagunaires du Rhône et son delta durant l'Antiquité. Mobilité environnementale et dynamiques géomorphologiques comme contraintes à l'aménagement (ports d'Arles, Fos/Saint-Gervais, Ulmet).In: Sanchez, C., Jézégou, M.-P. (Eds.), *Les ports dans l'espace méditerranéen antique: Narbonne et les systèmes portuaires fluvio-lagunaires, actes du colloque international tenu à Montpellier du 22 au 24 mai 2014*. Supplément. *Revue archéologique de Narbonnaise* **44**, 353–368. HAL ID: halshs-01957519.

Vella, C., Tomatis, C., Sivan, O., 2014. Chapitre 3. Le contexte de l'épave LE CONTEXTE PALÉOENVIRONNEMENTAL. *Archaeonautica*. HAL ID: hal-01435436.

Wright, L.D., 1977. Sediment transport and deposition at river mouths: a synthesis. *Geological Society of America Bulletin* **88**, 857–868.

Yuill, B.T., Khadka, A.K., Pereira, J., Allison, M. A., Meselhe, E.A., 2016. Morphodynamics of the erosional phase of crevasse-splay evolution and implications for river sediment diversion function. *Geomorphology* **259**, 12–29

Zolezzi, G., Luchi, R., Tubino, M., 2012. Modeling morphodynamic processes in meandering rivers with spatial width variations. *Reviews of Geophysics* **50**.